Sedimentary Geology 505 (2026) 107186

Contents lists available at ScienceDirect

Sedimentary Geology

journal homepage: www.elsevier.com/locate/sedgeo

A comparative study of methods for quantifying sand-sized sediment grain textural parameters

Xiaotian Shen [a], Xing Jian [a,*], Wei Zhang [a], Ruolan Liao [a], Dongming Hong [a], Chao Li [a], Shaohua Zhao [b], James T. Liu [c], Yuan-Pin Chang [c]

[a] State Key Laboratory of Marine Environmental Science, College of Ocean and Earth Sciences, Xiamen University, Xiamen, 361102, PR China
[b] Laboratory of Ocean and Coast Geology, Third Institute of Oceanography, Ministry of Natural Resources, Xiamen, 361005, PR China
[c] Department of Oceanography, National Sun Yat-sen University, Kaohsiung, 80424, Taiwan

ARTICLE INFO

Editor: Catherine Chagué

Keywords:
Sand-sized sediment
Grain texture
Grain size
Roundness
Sorting

ABSTRACT

Grain texture (including grain size and shape) is a fundamental property of sediments and provides critical information on sediment transport mechanisms, depositional environments, and post-depositional processes. Two-dimensional digital image analysis has been widely used to quantify textural parameters of unconsolidated sands and sandstones. However, standardized analytical workflows remain lacking. In this study, ten grain size descriptors and two roundness quantification methods were applied to measure the texture of 16 sand-sized samples from fluvial, aeolian, beach, and continental shelf environments. The effects of sample pretreatment procedures (cut versus uncut) and grain shape (granular quartz versus platy lithics) on quantification results were systematically evaluated. Results show that grain sizes measured from cut samples are generally smaller than those from uncut samples. For uncut samples, the Minor, Width, Minimum Feret, and equivalent spherical diameter correlate well with sieve-derived grain sizes, whereas the Major, Length, and Maximum Feret show good correspondence for cut samples. Grain roundness and sorting are influenced by pretreatment procedures, with cut samples generally exhibiting higher roundness but poorer sorting compared to uncut samples. Grains with high aspect ratios yield relatively lower accuracy, indicating controls of grain shape on the size quantification. We propose a practical workflow for selecting appropriate grain size descriptors for different sand types and provide a correction approach for converting two-dimensional grain size into three-dimensional data. This work improves texture quantification methodology of sand-sized sediments and provides methodological support for grain texture-related research in various disciplines of geosciences.

1. Introduction

Grain texture is a fundamental parameter for characterizing clastic sediments and sedimentary rocks, as it preserves critical information on transport processes, depositional environments, and post-depositional modifications (Vandenberghe, 2013; Vandenberghe et al., 2018; Reynolds, 2024). Therefore, determination of sediment grain texture has long been a central focus in geoscience research (Varga et al., 2018). Detrital grain texture of sediment (e.g., size and shape) exerts a primary control on sediment settling through hydraulic sorting (Rubey, 1933; Garzanti et al., 2009; Deal et al., 2023), and is therefore widely used in interpreting sedimentary environments (Campaña et al., 2016; Újvári et al., 2016; Shang et al., 2018). Furthermore, grain texture provides valuable constraints for interpretation of sediment transport and provenance (Mazzullo and Ritter, 1991; Woronko et al., 2017; Chmielowska et al., 2021), reservoir characterization (Payton et al., 2022; Yan et al., 2023; Murtaza et al., 2025), and geotechnical and geoengineering applications (Altuhafi et al., 2016; Xie et al., 2020; Wu et al., 2021).

In many sedimentological case studies, descriptions of sand-sized sediment texture remain qualitative and are commonly based on visual comparison charts (e.g., Muhlbauer et al., 2017; Woronko et al., 2017). Nevertheless, quantitative characterization of grain texture has been proven to be essential (Shen et al., 2024), yet a standardized and cost-effective procedure for such quantification is still lacking. Various techniques exist for measuring grain texture based on different principles. For unconsolidated sediments, sieving and laser diffraction are the most widely used methods (Folk, 1980; Konert and Vandenberghe,

* Corresponding author.
E-mail address: xjian@xmu.edu.cn (X. Jian).

https://doi.org/10.1016/j.sedgeo.2026.107186
Received 21 May 2026; Received in revised form 18 August 2026; Accepted 25 August 2026
Available online 27 August 2026

1997). Sieving is commonly applied to sand-sized fractions and primarily reflects the intermediate particle dimension, as grains tend to orient themselves optimally to pass through the mesh (Ludwick and Henderson, 1968; Varga et al., 2018). Laser diffraction, typically performed by a laser particle sizer, defines grain size as the diameter of an equivalent sphere (Konert and Vandenberghe, 1997) and is more suitable for fine-grained sediments, such as silt- and clay-sized grains. However, both methods provide only mass and volumetric distribution within different size fractions of bulk samples, rather than accurate size measurements of individual grains. Moreover, they are impractical for grain size analysis of ancient sandstones, owing to the difficulty of fully disaggregating hard rocks. In addition, the various components of sandstones, such as framework grains, matrix, and cement, which differ in origin and formation mechanisms, are difficult to analyze separately using these bulk techniques.

In recent years, digital image-based grain size analysis has been increasingly adopted (e.g., Perlo et al., 2016; Vandel et al., 2020), as it enables simultaneous quantification of grain size and shape parameters (e.g., roundness, aspect ratio, circularity, convexity) at the single-grain scale. In digital image processing, two-dimensional (2D) projections of grains are commonly used, and grain sizes are defined by various mathematical descriptors (Sochan et al., 2015; Anusree and Latha, 2023), such as equivalent spherical diameter and the equivalent area circle diameter (Hamzeloo et al., 2014; Bagheri et al., 2015). With advances in scanning technologies, three-dimensional (3D) grain images can also be obtained using techniques, such as 3D laser scanning, X-ray micro-computed tomography (μCT), and scanning electron microscope (SEM) micro-CT (Sun et al., 2014; Xie et al., 2020; Li et al., 2023). Recent comparative studies have systematically evaluated the performance of various grain-size characterization techniques, including 2D image analysis and 3D techniques (Houghton et al., 2024). Using spherical silica particles as the analytical material, the results demonstrated that grain size influences the accuracy of the analysis methods. For grains with diameters higher than 150 μm, X-ray computed tomography, as a 3D analysis method, provides the most accurate measurements, whereas laser diffraction tends to overestimate, and 2D automated image analysis and optical point counting tend to underestimate (Houghton et al., 2024). However, 2D digital image analysis is more practical and cost-effective than 3D measurements. Furthermore, as mentioned above, sandstones contain components of different origins and are therefore routinely cut into thin sections for petrographic analysis under a polarizing microscope, providing 2D images that can be used for both textural and compositional analysis (Weltje and von Eynatten, 2004).

Numerous mathematical descriptors based on 2D digital images have been proposed for measuring grain texture (Anusree and Latha, 2023). Because these descriptors are defined differently, they can yield significantly different results for the same grains, particularly for irregular grains, and different descriptors are optimal for different particle types. For example, the equivalent spherical diameter (ESD), which assumes that grains are approximately spherical, is widely used for sand-sized grains (Garzanti et al., 2008; Lawrence et al., 2011), as sediment grains are often idealized as spheres in many sedimentological studies. Despite the broad adoption of these descriptors, several challenges hinder the application of digital image processing. First, a single grain can produce an infinite number of possible 2D projections (Xie et al., 2020), and the measured size therefore depends strongly on both the projection selected and the method used. This issue is compounded by differences in pretreatment procedures between unconsolidated sediments and sandstones. Second, no single metric is universally accepted for representing the size of grains with different shapes, because particle morphology can significantly affect texture quantification (Varga et al., 2018). Sand-sized detrital grains exhibit diverse shapes, such as granular (e.g., quartz, garnet), columnar or platy (e.g., zircon, mica, and metamorphic lithics), raising questions about the suitability of a single metric for all grain types. Third, although many studies have sought to establish relationships between 2D and 3D measurements (e.g., Xie et al., 2020), the extent to which 2D grain images represent true 3D particle geometry remains uncertain. Consequently, these issues highlight the need for further investigations into the application of 2D digital image processing for quantifying the texture of sand-sized sediments.

In this study, grain textural parameters (grain size, sorting, and roundness) of sand-sized sediments from different sedimentary environments (including fluvial, aeolian, beach, and continental shelf sands; Table 1) were measured using multiple quantification methods via 2D digital image processing. These methods include equivalent spherical diameter, equivalent area circle diameter, equivalent perimeter circle diameter, maximum Feret, minimum Feret, diameter of maximum inscribed circle, major and minor axes of best-fit ellipse, and length and width of best-fit rectangle for grain size, and the Wadell's and Pentland's roundness (Table 2). Images from cut (thin section) and uncut (original) grains were also compared. The objectives of this study are 1) to determine the influence of thin section cutting on the quantification of grain textural features; 2) to compare the accuracy of quantification methods; and 3) to identify the optimal quantification methods for unconsolidated sands and sandstones from different sedimentary environments.

2. Geological setting and samples

A total of 16 reference sand samples were collected from four depositional environments in southeastern China, including eight river sands, four continental shelf sands from the Taiwan Strait, two old red sands, and two beach sands (Fig. 1B). The bedrock lithology and river drainage systems on the eastern and western sides of the Taiwan Strait differ markedly (Fig. 1) (Shen et al., 2021). The southeastern China mainland, on the western side of the strait, is predominantly composed of intermediate-acid igneous rocks, volcanic rocks, and volcano-sedimentary rocks of Jurassic to Cretaceous age (Fig. 1C–D) (Li et al., 2014). Many rivers drain this region (Fig. 1B), including large rivers (e.g., Pearl River), mesoscale rivers (e.g., Minjiang, Hanjiang, and Jiulongjiang Rivers), and small rivers (e.g., Zhangjiang and Jinjiang Rivers). In contrast, Taiwan Island consists mainly of Cenozoic sedimentary rocks and Mesozoic (meta)sedimentary rocks (Fig. 1C) (Huang, 2017). Tens of small mountainous rivers, such as the Zhuoshui and Gaoping Rivers, flow westward into the Taiwan Strait and the South China Sea (Fig. 1B). The Taiwan Island is tectonically active owing to the subduction-collision between the Philippine Sea Plate and the Eurasian continent. Due to these distinct geological settings, river sediments from the two regions exhibit remarkable compositional diversity (Shen et al., 2021). The Taiwan Strait is spatially diverse in topography and comprises two conjugated tidal erosional and depositional systems, including the Taiwan Shoal and the Wuchu Depression, and the Changyun Ridge and the Penghu Channel. This diversity is thought to influence the sediment transport and composition in the strait (Shen et al., 2021). The old red sand is a red or brownish-red, partially-cemented fine- to medium-grained sand formed in aeolian environments under the influence of the Asian monsoon and eustasy (Jin et al., 2017) and is widely distributed along the southeastern coast of China (Xu et al., 2024).

On the basis of petrographic composition of the 63–500 μm size fraction (data from Hong, 2020; Shen et al., 2021; Zhang et al., 2022 and unpublished data), these samples were classified into three groups (Fig. 2): six quartz-rich samples (A1–A6, A14, and A15) characterized by high quartz and low lithic contents (Fig. 3A–C); six mixed samples (A7–A11 and A18) with high abundances of both quartz and lithic fragments (Fig. 3D–F); and four lithics-rich samples (A12, A13, A16, and A17) dominated by lithic fragments (Fig. 3G–I). The two old red sand samples (A1 and A2/3) are silty fine-grained sand and medium-coarse sand, collected from two outcrop sections at Zhanjiang and Pingtan, respectively (Fig. S1 in Appendix A). Samples A4 and A5/6 are coarse sands collected from two littoral sandy beaches in Zhaoan Bay and at the Jinjiang River estuary. Beach samples were collected from the foreshore

Table 1
Information on analyzed samples in this study, including sample description, location, target grain size range and petrographic composition.

Type	Sample name	Sample_ID	Description	Location	Grain size		Petrographic composition (%) in 63–500 μm fractions			Petrographic composition (%) in the texture-quantified fractions		
					(Mesh)	(μm)	Q	F	L	Q	F	L
Quartz-rich	DMX-01	A1	Old red sand	Zhanjiang, Guangdong	60–70	220–300	82.6	10.4	7.0	96.1	0.0	3.9
	QF-06	A2	Old red sand	Pingtan, Fujian	60–70	220–300	57.3	28.4	14.3	82.7	7.4	9.9
	QF-06	A3	Old red sand	Pingtan, Fujian	120–150	100–125	57.3	28.4	14.3	84.5	4.8	10.7
	FJHT-103	A4	Beach sand	Zhaoan Bay, Fujian	40–50	355–450	81.9	15.8	2.3	96.5	0.0	3.5
	FJHT-086	A5	Beach sand	Jinjiang River Estuary	50–60	300–355	85.4	10.2	4.4	87.0	0.0	9.9
	FJHT-086	A6	Beach sand	Jinjiang River Estuary	40–50	355–450	85.4	10.2	4.4	85.6	12.0	2.4
	B4	A14	Continental shelf sand	Taiwan Strait	50–60	300–355	81.6	8.2	10.1	92.6	0.0	7.4
	HS2–6	A15	Continental shelf sand	Taiwan Strait	50–60	300–355	81.9	9.2	8.9	90.1	0.0	9.9
Mixed	19ZJ-08	A7	River sand	Zhangjiang River	90–120	125–160	47.5	16.0	36.5	66.0	14.8	19.2
	19JJ-13	A8	River sand	Jinjiang River	90–120	125–160	53.8	15.9	30.3	71.9	10.8	17.2
	19FD-13	A9	River sand	Tongshanxi River	60–70	220–300	29.1	11.2	59.7	8.7	2.4	88.9
	19JX-06	A10	River sand	Jiaoxi River	60–70	220–300	35.8	21.0	43.2	45.0	19.0	36.0
	C6	A11	Continental shelf sand	Taiwan Strait	90–120	125–160	63.1	6.9	30.0	69.8	5.9	24.3
	Y33	A18	Continental shelf sand	Taiwan Strait	120–150	100–125	41.0	5.5	53.5	66.0	14.8	19.2
Lithics-rich	JRD-11	A12	River sand	Zhuoshui River	50–60	300–355	6.8	12.4	80.8	13.0	2.0	85.0
	JRD-10	A13	River sand	Zhuoshui River	60–90	160–300	15.9	16.4	67.7	20.0	3.5	76.5
	JRD-13	A16	River sand	Zhuoshui River	90–120	125–160	16.6	18.1	65.3	54.8	0.0	45.2
	JRD-28	A17	River sand	Zhuoshui River	120–150	100–125	4.2	16.1	79.7	20.4	0.0	79.6

Table 2
Definitions of quantification methods for grain size and roundness.

Quantification methods	Symbols	Definitions
Grain size		
Equivalent spherical diameter	ESD	ESD equals $(X*Y*Z)^{1/3}$; X, Y, Z for short, intermediate, long axes of particle
Equivalent area circle	ArEquivD	Diameter of circle with the same area as the particle
Equivalent perimeter circle	PerEquivD	Diameter of circle with the same perimeter as the particle
Feret	Max Feret; Min Feret	Distance between two tangents on opposite sides of the particle; Maximum feret, Minimum feret
Maximum inscribed circle	MinR	Diameter of maximum inscribed circle of the particle
Best-fit ellipse	Major; Minor	Major and Minor axes of the ellipse with smallest area that fits around the particle
Best-fit rectangle	Length; Width	Length and Width of the rectangle with smallest are that fits around the particle
Roundness		
Wadell	Rw	Average radius of curvature of all corners of the grain in one section divided by the radius of the largest inscribed circle in that section
Pentland	Rs	Rs equals $4*A/(\pi*L_{Major}^2)$, A for projection area of particle, L_{Major} for maximum axis of particle

zone (Fig. S1). Samples A14 and A15 are quartz-rich coarse sands from the Taiwan Shoal, a shallow region with an average water depth of 20 m in the southern Taiwan Strait. Two other continental shelf samples (A11 and A18) are fine-grained sands from the south margin of the Taiwan Shoal and the middle Taiwan Strait, respectively. Four mixed samples (A7, A8, A9, and A10) are fine- to medium-grained sands collected from the floodplains of four small rivers, e.g., the Zhangjiang, Jinjiang, Tongshanxi, and Jiaoxi Rivers (Fig. S1). The lithics-rich samples (A12, A13, A16, and A17) are fine- to coarse-grained sands from the upper 15 m of a sediment core (JRD-N) in the Zhuoshui River estuary, deposited in a deltaic environment since the Holocene (Yang et al., 2017; Zhang et al., 2022).

3. Methodology

3.1. Sample pretreatment

For petrographic analysis, each sample was wet-sieved through a 230-mesh sieve to obtain the >63 μm fraction and then dried. This fraction was dry-sieved through a 35-mesh sieve to separate the 63–500 μm fraction, which was subsequently impregnated with Araldite and cut into standard thin sections (0.03 mm thick). Modal compositions (quartz, feldspar, and lithic fragments) were determined using the Gazzi-Dickinson point-counting method (Dickinson and Suczek, 1979; Dickinson, 1985).

To quantify the accuracy of different texture-quantification methods, the 63–500 μm fraction of each sample was further dry-sieved using a series of mesh sizes (40, 50, 60, 70, 80, 90, 100, 120, and 150) to obtain grains within narrow grain size windows. The size fraction with the highest content in each sample was selected as the target grain size window for further textural analysis. Each sample was assigned a single target grain size window, except for samples QF-06 and FJHT-086 (Table 1). Each sample was then divided into two aliquots prepared for two different pretreatment procedures. One aliquot was impregnated with Araldite and cut into standard thin sections. These samples are referred to as "*cut samples*" in this paper. The other aliquot was gently transferred onto a microscope slide using a soft brush, and the slide was lightly tapped to minimize grain overlap and ensure stable grain orientations. Samples treated by this method are referred to as "*uncut samples*". In total, eighteen uncut and eighteen cut samples were obtained. The modal compositions of cut samples were also determined by using the Gazzi-Dickinson point-counting method. The petrographic compositions of all samples in the 63–500 μm fraction and in the analyzed grain size window are plotted in the Q-F-L ternary diagram (Fig. 2).

3.2. Digital image processing

Eighteen thin sections (cut samples) and eighteen slides (uncut samples) were imaged using a polarizing microscope under plane-polarized light to obtain two-dimensional images of the analyzed grains. All images were acquired at a resolution of 1600 × 1200 pixels. To reduce uncertainties arising from the image-analysis workflow (Anusree and Latha, 2023), we applied a uniform image-processing workflow for all images. All images were processed using the software

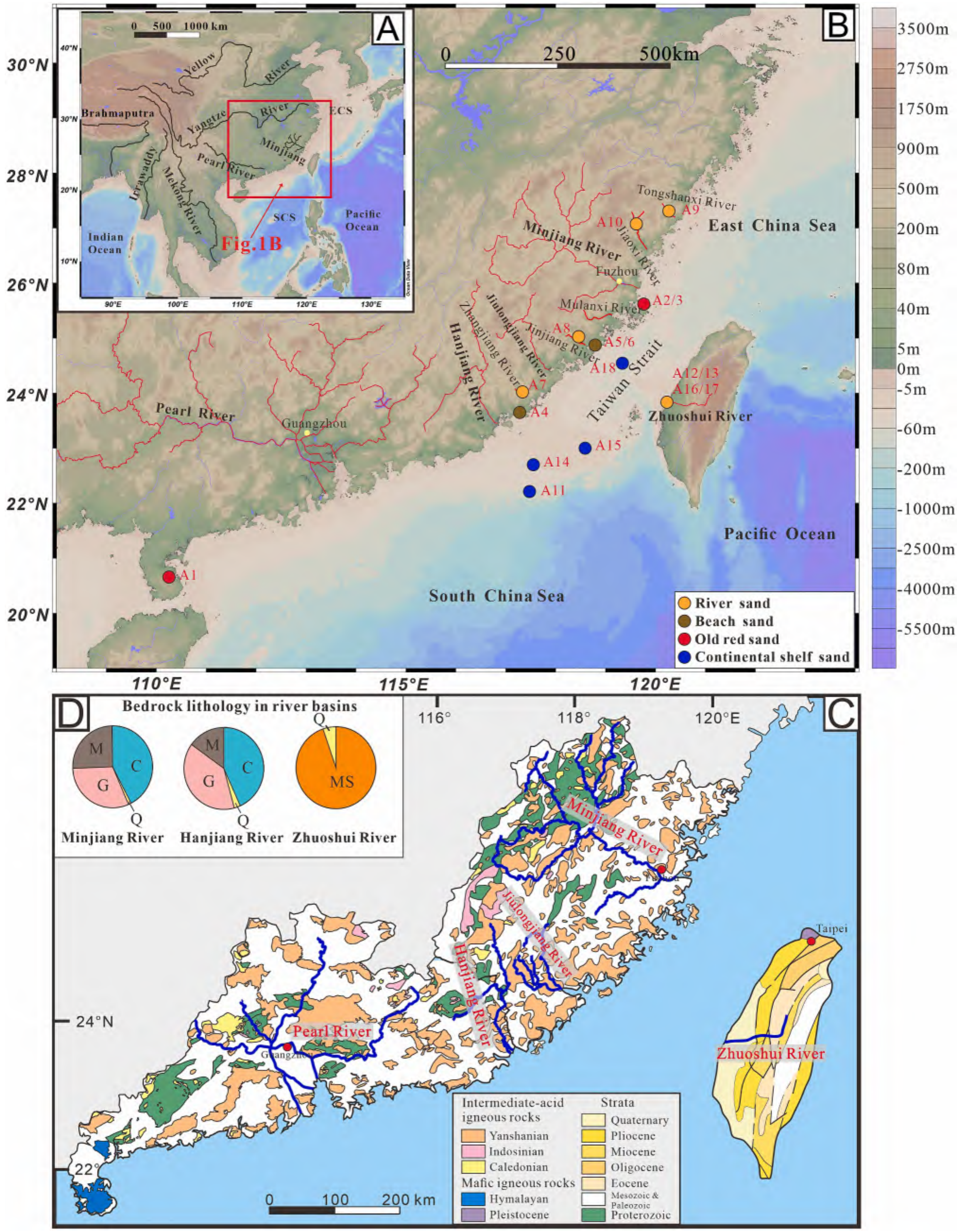

Fig. 1. Location and geological background of the study area. (A) Background of southeastern China and major rivers in East Asia. (B) Locations of analyzed samples in this study and major rivers in southeastern China. Different types of sediments are marked by different symbols. (C) Geological map of South China (modified from Institute of Geology, Chinese Academy of Geological Sciences, 2002) and large rivers in South China. (D) Quantified lithology in river basins according to Wang et al. (2024). C, Q, G, M, and MS represent clastic sedimentary rocks, Quaternary sediments, intermediate-acid igneous rocks, metamorphic rocks, and meta-sedimentary rocks, respectively.

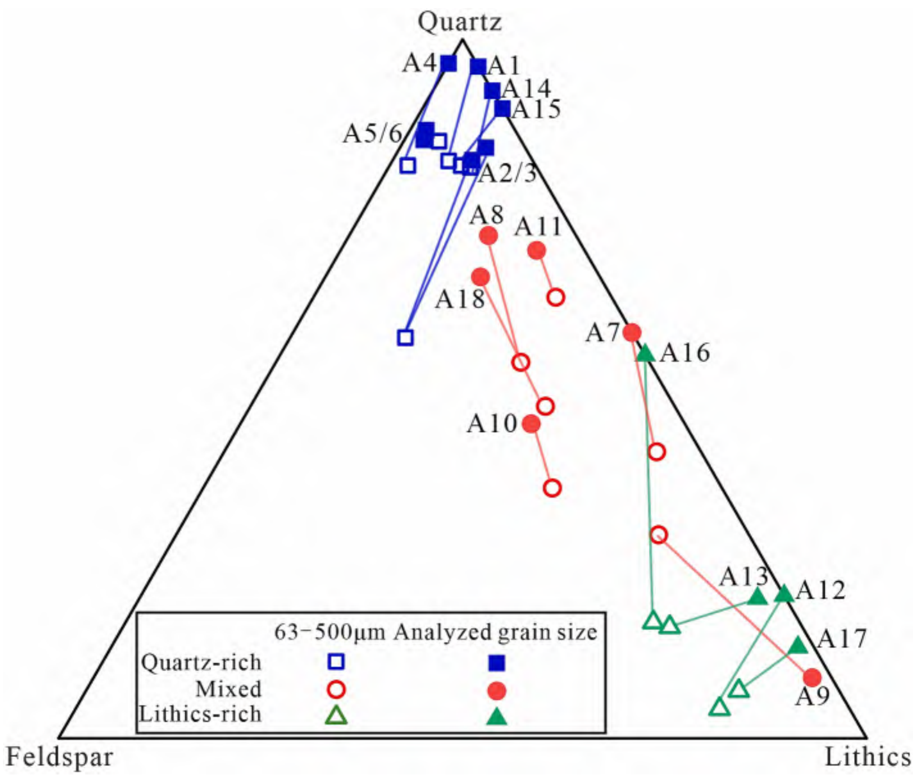

Fig. 2. Modal analysis results of sand framework grain compositions. Each sample has two sets of data, including modal compositions of the 63–500 μm fraction (hollowed) and the analyzed grain size fraction (filled) of all samples.

ImageJ with a batch macro to generate binary images followed by image sharpening, denoising, eroding, and manual removal of overlapping particles. The binary images were then analyzed in the software Matlab using a uniform script to quantify grain size and roundness of each grain. Overlapping grains were manually excluded from the measurements. Grain size was determined using the *Image Processing Toolbox*, and grain roundness was calculated using a script from Resentini et al. (2018). For each sample, approximately 500 grains from each uncut sample and 200 grains from each cut sample were randomly selected for analysis.

3.3. Granulometry

Grain size is one of the most fundamental physical properties of detrital grains, and its distribution directly reflects transport mechanisms, depositional hydrodynamic conditions, and provenance information, making it an indispensable parameter in sedimentological research. In this study, ten commonly used grain size descriptors were evaluated (Fig. 4; Table 2), including equivalent spherical diameter (ESD), equivalent area circle diameter (ArEquivD), equivalent perimeter circle diameter (PerEquivD), maximum Feret (Max Feret), minimum Feret (Min Feret), diameter of maximum inscribed circle (MinR), major and minor axes of the best-fit ellipse (Major and Minor), and length and width of best-fit rectangle (Length and Width). The definitions and calculation methods of these descriptors are provided in Table 2.

To evaluate the accuracy of each method, we defined an ‘accuracy’ index as the ratio of the number of grains with measured sizes falling within the reference mesh range to the total number of measured grains. It should be noted that the upper limit of the reference mesh range was corrected to the diagonal of a square sieve because particles can pass through the diagonal of a sieve (Kumara et al., 2012).

3.4. Grain roundness measurement

Roundness of grains is an important sedimentological parameter that reflects the mechanical and chemical abrasion experienced by grains during transport and sedimentation. In earlier literature, there were two distinct definitions and quantification methods: one referred to the degree of rounding of grain corners and edges (Wadell, 1932), and the other described the overall extent to which a grain approaches a circle or sphere (Pentland, 1927). Although the latter adopted the term ‘roundness’ in the literature, it is now widely recognized that its actual definition corresponds to circularity or sphericity (Anusree and Latha, 2023). In this study, we applied two grain roundness quantification methods (Fig. 4; Table 2), including the Wadell's method (Wadell, 1932) and the Pentland's method (Pentland, 1927), the latter of which was used in the software ImageJ (Cox and Budhu, 2008). The Wadell's roundness (Rw) defines grain roundness as the average radius of curvature of all corners of the grain projection divided by the radius of the largest inscribed circle. The Pentland's roundness (Rs) is defined as $4*A/(\pi*L_{Major}^2)$, where A is the area and L_{Major} is the major axis length of the grain projection.

3.5. Sorting calculation

Sediment sorting is closely linked to the sedimentary environment and hydraulic sorting conditions during deposition. The sorting index of each sample was quantified as the relative standard deviation of grain sizes of all the measured grains (Shen et al., 2025). For each cut and uncut sample, ten sorting values were calculated, corresponding to the ten grain size descriptors. Because the analyzed grains fall within a narrow size range after mesh sieving, the analyzed samples should be well sorted. Based on this assumption, the sorting calculations can be used to evaluate the performance of different grain size quantification methods.

3.6. Scanning electron microscopy

To provide a partial three-dimensional characterization of grain

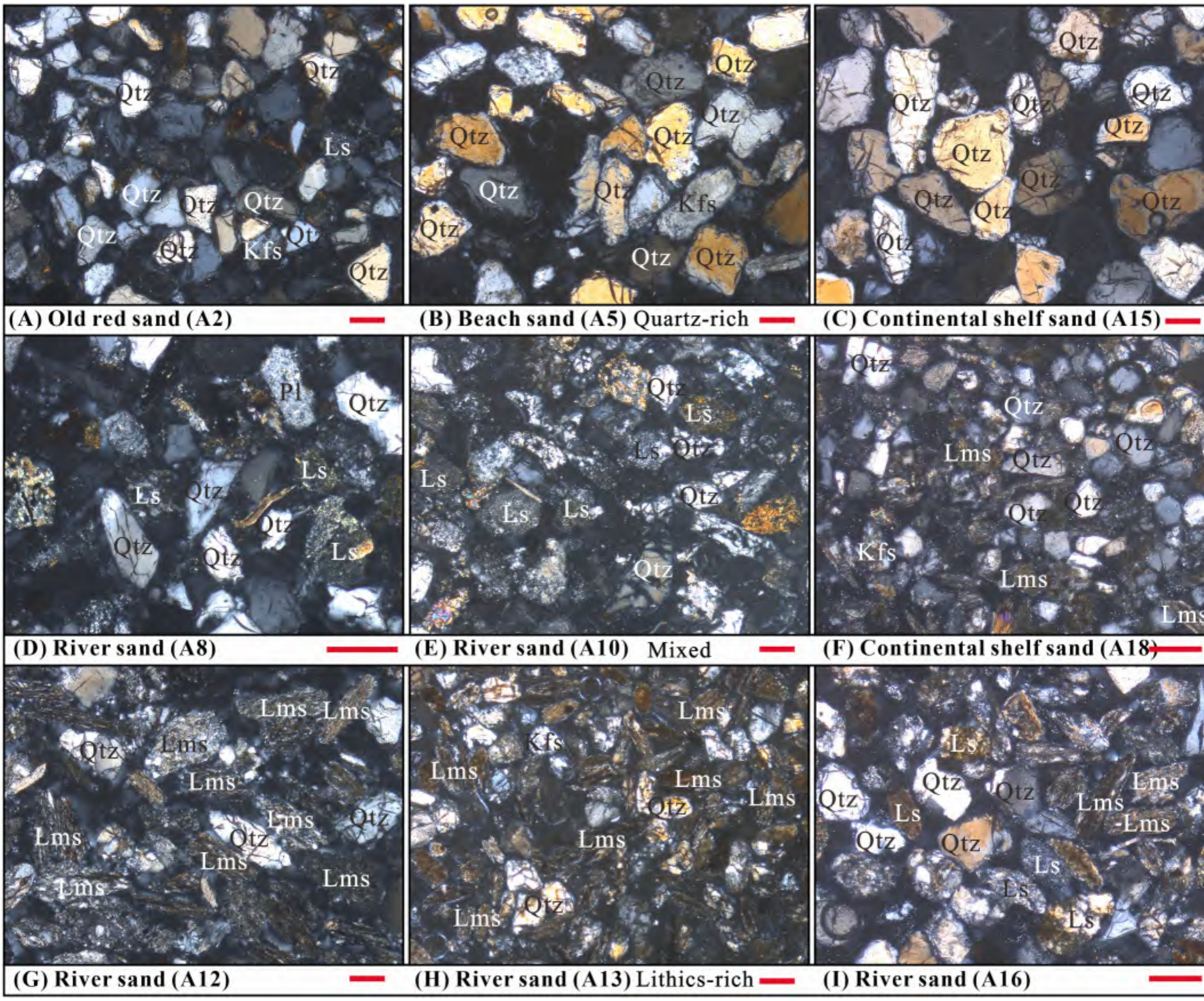

Fig. 3. Representative photomicrographs of samples treated by the cut method. (A–C) Quartz-rich samples, including old red sand from Pingtan Island (A), beach sand from the Jinjiang River estuary (B), and continental shelf sand from the Taiwan Strait (C). (D–F) Mixed samples, including Jinjiang River sand (D), Jiaoxi River sand (E), and continental shelf sand from the Taiwan Strait (F). (G–I) Lithics-rich samples from the Zhuoshui River. Abbreviations in the figure: Qtz-quartz; Kfs-K-feldspar; Pl-plagioclase; Ls-sedimentary lithic fragment; Lms: metasedimentary lithic fragment. Red bars represent 200 μm in all photos.

texture, six samples (A2, A5, A10, A13, A15, and A18) were selected for scanning electron microscopy (SEM) analysis. These samples encompass various sediment types (Table 1). The analytical procedure followed Cox and Budhu (2008). For each sample, more than 100 grains were randomly selected, mounted on carbon tape affixed to SEM stubs, and then gold-coated to enhance the signal of sand grains. SEM imaging was conducted using a scanning electron microscope (Quanta 650, FEI Inc.) at Xiamen University under secondary electron mode with an accelerating voltage of 5 kV. Magnification was adjusted to capture one or several entire grains within each image.

4. Results

4.1. Comparison of cut and uncut detrital grains

The images of the same sample derived from cut, uncut, and SEM analyses reveal considerable differences (Fig. 5). For sample A2 (quartz-rich old red sand), the uncut image shows that grains are mainly composed of well-rounded, subrounded to subangular grains with a mean ESD of 204.39 μm and a sorting of 0.2920 (Fig. 5A). The cut image exhibits a smaller mean ESD of 179.83 μm (sorting 0.2988) than uncut image (Fig. 5B). The SEM image reveals that most grains are granular with relatively rough surfaces (Fig. 5C). For sample A10 (river sand), the uncut image displays subrounded to rounded grains with a mean ESD of 231.10 μm and a sorting of 0.2944 (Fig. 5D). The cut image shows irregular edges and angular grains, with a smaller mean ESD of 201.15 μm (sorting 0.2647) than uncut image (Fig. 5E). The SEM image indicates that grains are generally subangular to subrounded, with irregular outlines and some distinct angular edges (Fig. 5F). For sample A13 (lithics-rich river sand), the uncut image consists of well-sorted, subrounded to rounded grains (mean ESD 242.95 μm; sorting 0.1547) (Fig. 5G). The cut image displays pronounced differences compared with the uncut image and shows that grains are mostly angular and elongated, with a mean ESD reduced to 159.57 μm and sorting increased to 0.2623 (Fig. 5H). The SEM image shows that many grains of sample A13 are platy with laminated features and small thickness (Fig. 5I). These features explain the reason for large discrepancies between cut and uncut images. When the cutting orientation is perpendicular to the maximum projection plane of platy grains, the resulting 2D projection of the grains tends to be elongated, like grains in Fig. 5H. The SEM images

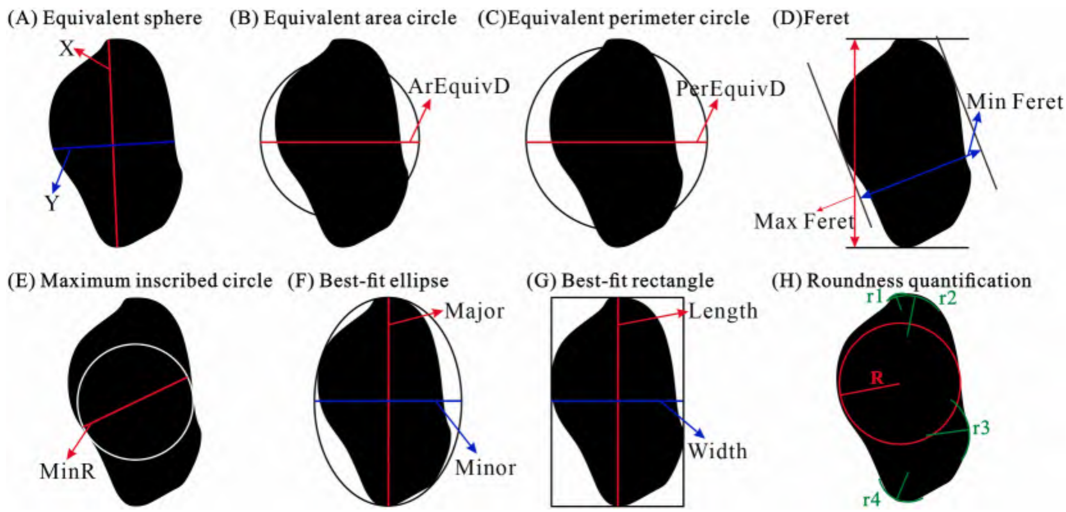

Fig. 4. Schematic diagram of quantification methods for grain size (A–G) and roundness (H, the Wadell's method). R and ri represent the radius of the maximum inscribed circle and the radii of inscribed circles in corners, respectively.

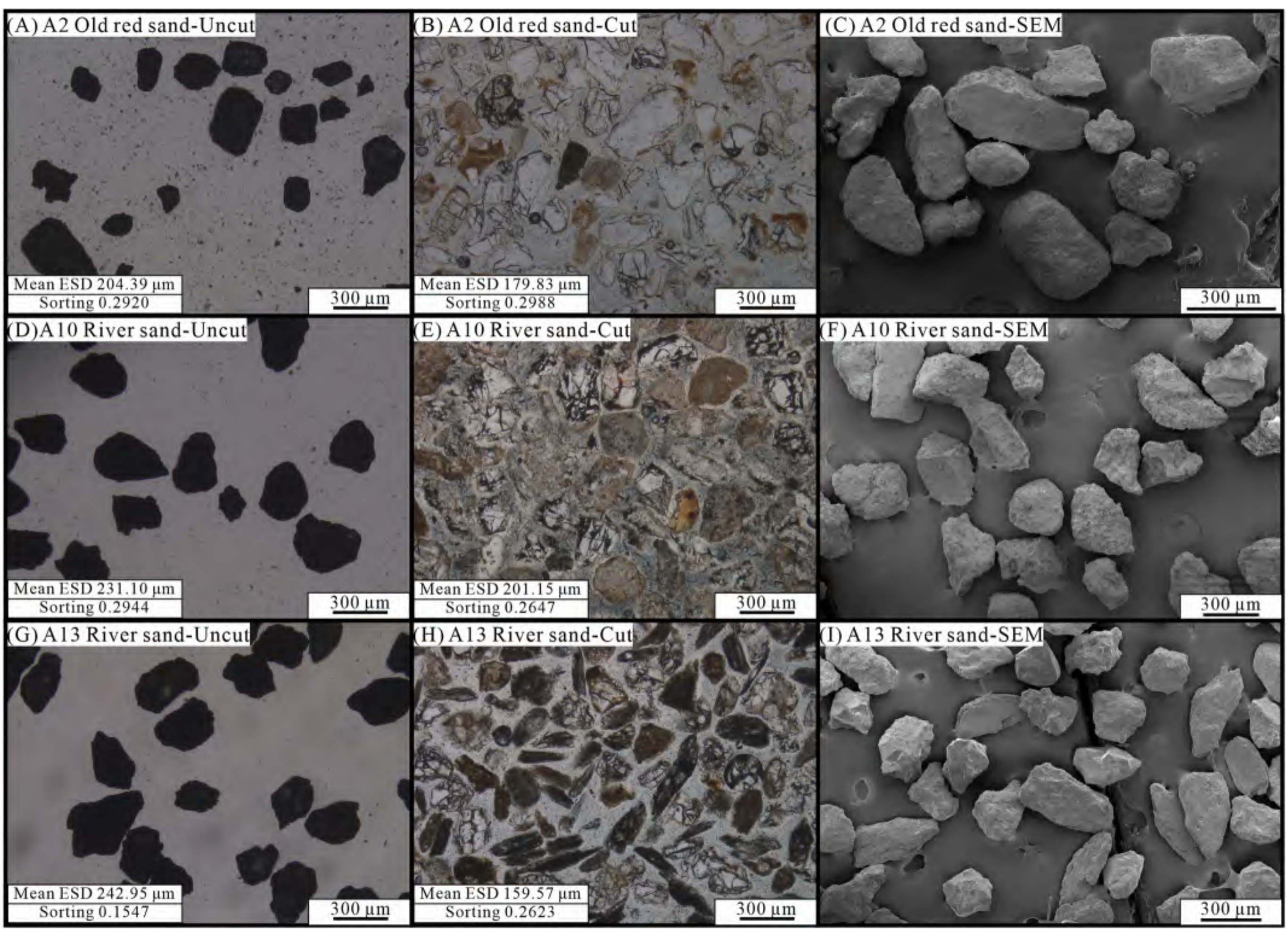

Fig. 5. Representative two-dimensional images of three types of sediments, including sample A2 (quartz-rich old red sand; A–C), A10 (mixed sand; D–F), and A13 (lithics-rich river sand; G–I). The left panel shows images of samples treated by the uncut method, and the middle panel shows those treated by the cut method. The right panel shows SEM images. Mean ESD size and sorting calculated from ESD sizes of samples are marked.

also reveal micro-fractures and surface textures that are not observable under optical microscopy, thus providing complementary three-dimensional information.

Comparison of cut and uncut samples indicates pronounced differences in grain size estimates (Fig. 6). These differences vary among the three types of sands. Grain sizes of most samples treated by the cut

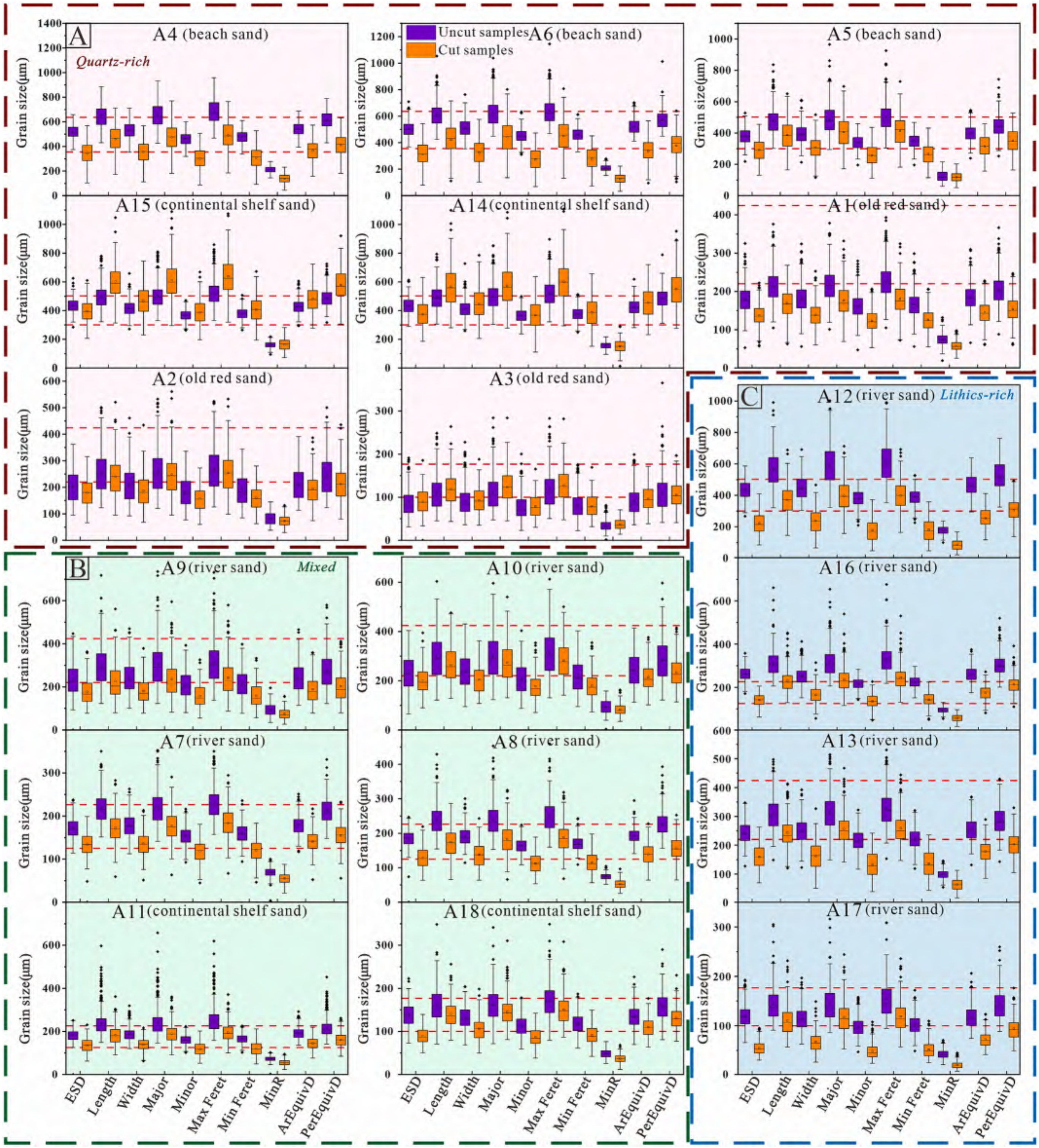

Fig. 6. Box plots of grain sizes of all samples and comparison between results of uncut and cut samples. (A) Quartz-rich samples; (B) Mixed samples; (C) Lithics-rich samples. Note that the maximum of the reference grain size range is the diagonal length of the square sieve. Red dashed lines in the charts represent the reference grain size range.

method are systematically smaller than those obtained by the uncut method across all ten grain size descriptors (Fig. 6). This pattern is observed in all six compositionally mixed samples and all four lithics-rich samples (Fig. 6B–C), as well as in several quartz-rich samples (A1 and A4–A6; Fig. 6A). In contrast, the continental shelf sands (A14 and A15) exhibit larger grain sizes in cut samples than in uncut grains for all quantification methods except the ESD and MinR methods (Fig. 6A). The old red sand samples (A2 and A3) show only minor differences between the two pretreatment methods (Fig. 6A). Notably, the quantified grain size distributions do not always correspond well to the mesh-defined size ranges (Fig. 6). Accuracy also differs between cut and uncut samples, with uncut samples generally showing higher accuracy than cut samples (Fig. 7). Specifically, 15 and 7 of the 18 uncut samples exhibit accuracies greater than 0.7 and 0.5, respectively, compared with 8 and 6 of the 18

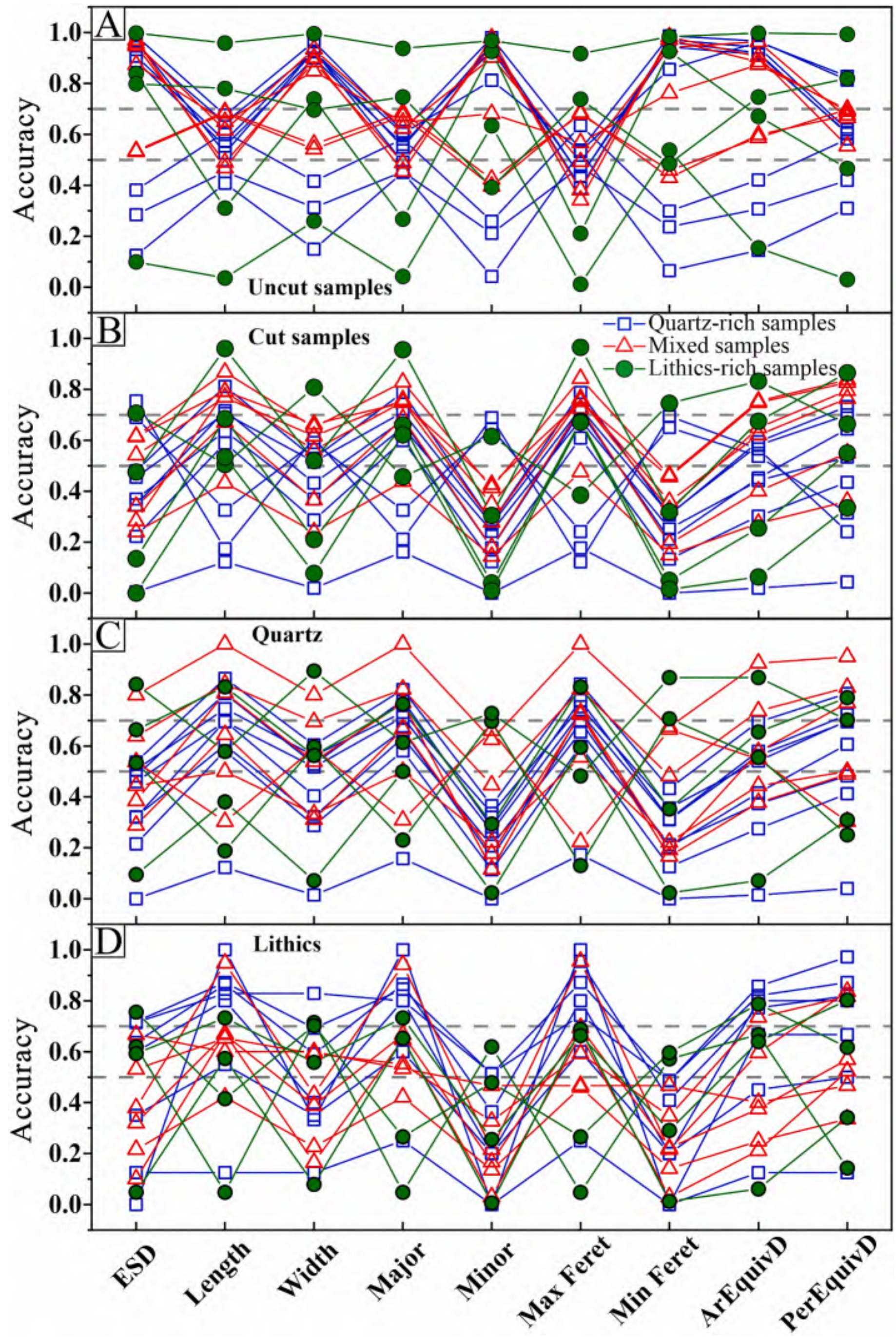

Fig. 7. Accuracy of ten grain size quantification methods and comparison between results of uncut samples (A) and cut samples (B), and between results of quartz (C) and lithics (D). The accuracy of each method was calculated as the ratio between the number of grains with grain size within the reference size range and the total number of measured grains. Two gray dashed lines mark accuracy values of 0.5 and 0.7, respectively.

cut samples.

The ten grain size descriptors yield systematically different results and exhibit variable measurement accuracies (Figs. 6, 7). As expected, the MinR method yields the smallest grain sizes because it is defined as the diameter of the largest inscribed circle within a grain. In contrast, the Length, Major, Max Feret, and PerEquivD methods generally produce larger values (Fig. 6), as they are controlled by the maximum grain dimension (Fig. 4). Conversely, the Width, Minor, and Min Feret methods yield smaller estimates because they reflect the second longest dimension of the grain. For uncut samples, the ESD and ArEquivD methods show the highest accuracy, with 14 samples exceeding 50% and 11 exceeding 70%. The Width, Height, Minor, and Min Feret show slightly lower accuracy, with about 12 samples exceeding 50% and 9 higher than 70%. In contrast, the Major, Max Feret and PerEquivD methods exhibit relatively low accuracy, with only 2, 2, and 4 of the 18 samples exceeding 70%, respectively. The accuracy of the MinR method is the lowest among all methods with all samples yielding zero accuracy. For cut samples, the Major, Max Feret, and PerEquivD methods are comparatively more reliable, with 12 samples exceeding 50% accuracy and 7 samples exceeding 70%. Other descriptors show lower accuracy, with fewer than 4 samples achieving accuracy greater than 70% (Fig. 7).

Sorting calculated from the quantified grain size data indicates that sample pretreatment significantly influences the derived sorting values (Fig. 8). For most samples, the cut method yields higher sorting indices

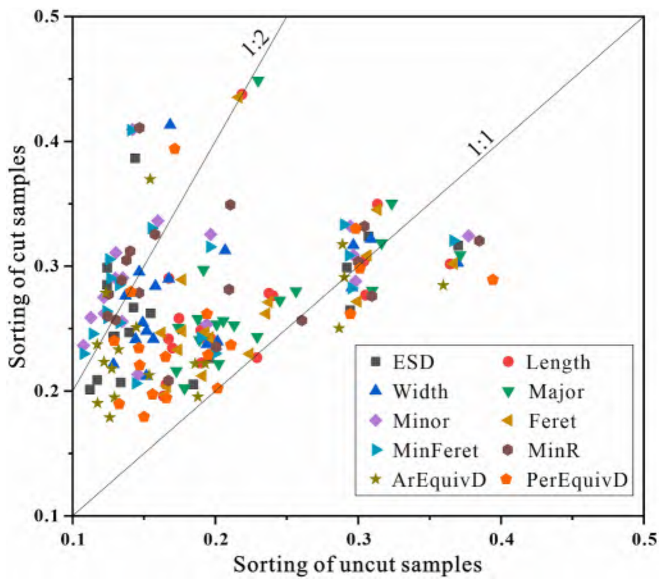

Fig. 8. Sorting of all samples, and comparison between cut and uncut samples and among ten grain size quantification methods. Two black lines represent ratios of 1:1 and 1:2.

than the uncut method (Fig. 8), a pattern observed for all ten grain size descriptors, albeit to varying degrees. The Minor, Width, and Min Feret show the largest ratios between uncut and cut samples, whereas the Major method is least affected by the different pretreatment procedures.

The quantified roundness values exhibit a consistent pattern across all samples (Fig. 9). When using the Wadell's method, all cut samples show systematically higher roundness than uncut samples, whereas the opposite trend is observed when roundness is calculated using the Pentland's method (Fig. 9). For the uncut samples, Rs values are generally higher than Rw values, whereas the relationship between Rs and Rw roundness is not consistent for cut samples (Fig. 9).

4.2. Comparison of measured quartz and lithic grains in cut samples

For most quantification methods, the measured sizes of quartz and lithic grains within the same sample differ. It is worth noting that the size differences between quartz and lithics are not consistent when different quantification methods are applied. For the four lithics-rich samples, when using the Length, Major, and Max Feret methods, which focus on the longest axes of grains, lithic grains are larger than quartz grains (Fig. 10C). Conversely, methods that measure the short axes (Width, Minor, and Min Feret) yield larger values for quartz grains than lithic grains. This pattern is reasonable because the aspect ratios of platy lithic grains are overestimated when using the cut method, leading to an increase in the long axis and a decrease in the short axis (Figs. 5G–H, 11). The mixed samples A11 and A18, which were collected from the Taiwan Strait and contain high abundances of metamorphic lithics similar to Zhuoshui River sediments (Shen et al., 2021), also exhibit a similar trend: lithic grains show larger Length, Major, and Max

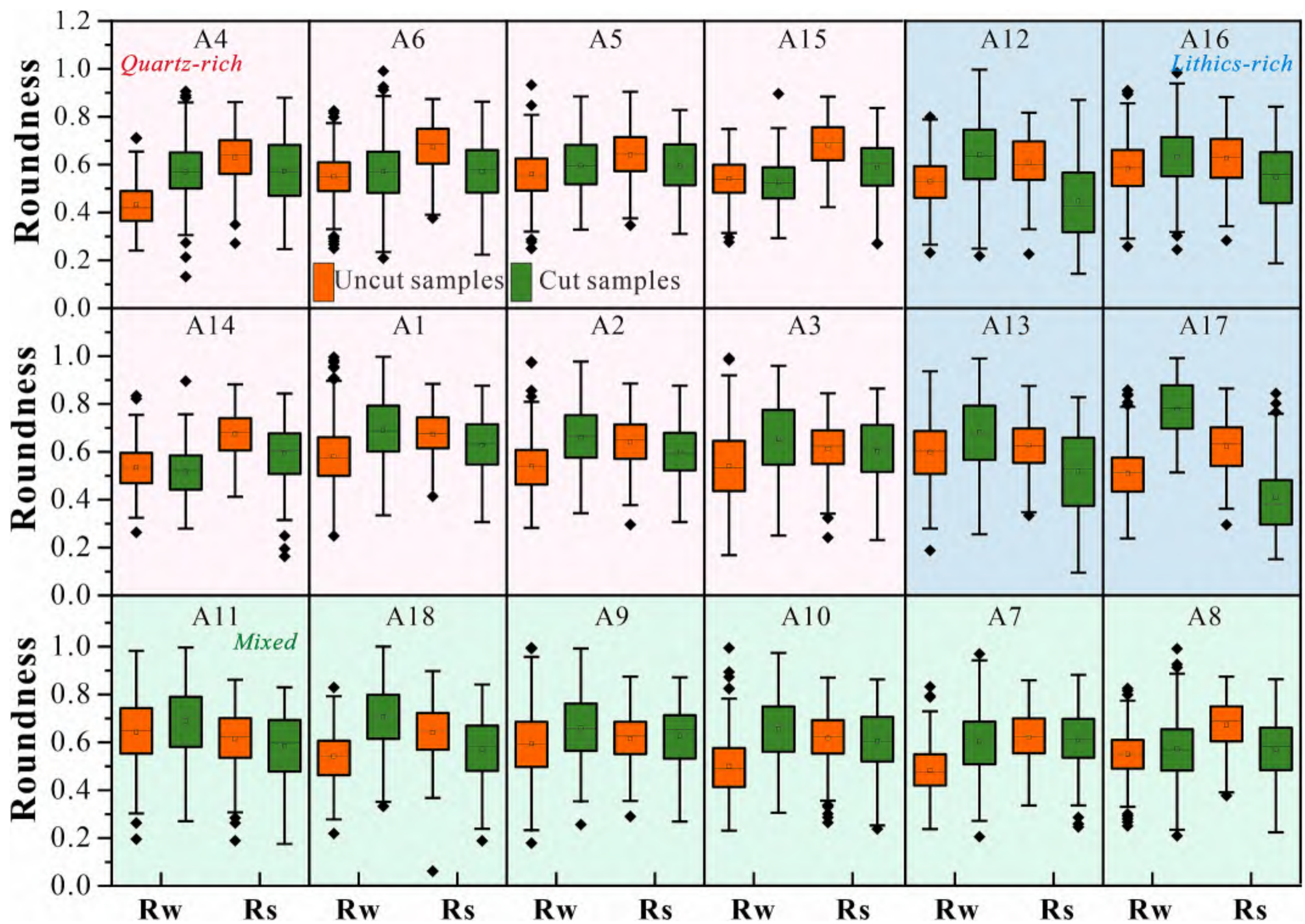

Fig. 9. Roundness of analyzed samples and comparison between uncut and cut pretreatment methods and between two quantification methods. Quartz-rich, lithics-rich, and mixed samples are shown in red, blue, and green boxes, respectively.

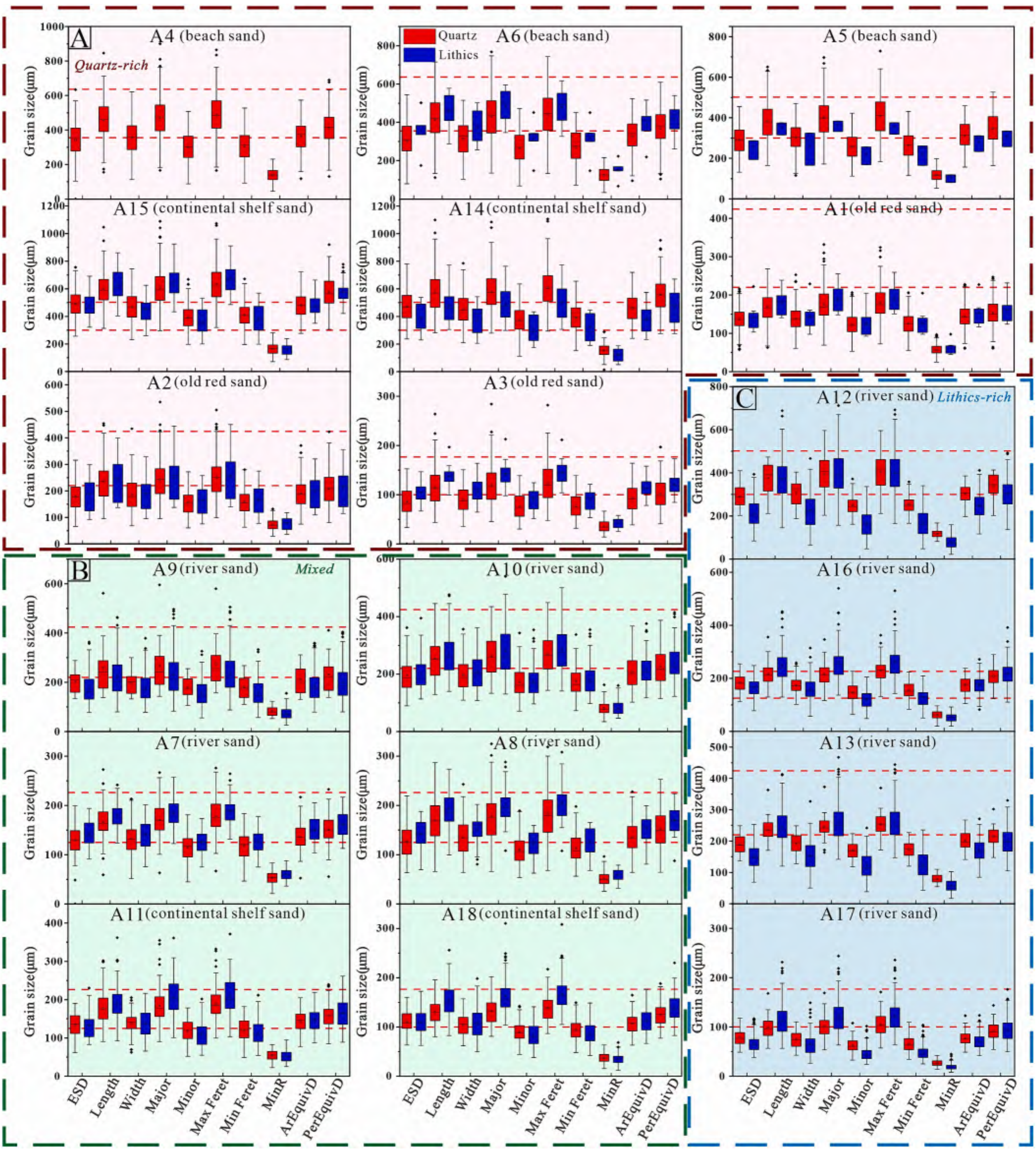

Fig. 10. Comparison between grain size quantification results of quartz and lithics in all samples. (A) Quartz-rich samples; (B) Mixed samples; (C) Lithics-rich samples. Red dashed lines represent the grain size range of meshes.

Feret sizes than quartz grains, whereas quartz and lithic sizes are comparable when other methods are applied. For other quartz-rich and mixed samples, the differences between quartz and lithic grains are not significant (Fig. 10A–B), despite the very low lithic content in the quartz-rich samples. Unlike the Zhuoshui River samples, the lithic fragments in Fujian mountainous river sediments consist mainly of sedimentary lithics (Fig. 3A–F), which are equant rather than elongated.

The ten quantification methods yield varying results and accuracies for quartz and lithics (Figs. 7C–D, 10). In general, the Length, Major, and Max Feret methods produce larger sizes than the ESD, Width, Minor, Min Feret, ArEquivD, and PerEquivD methods, whereas the MinR method yields the smallest sizes. Regarding accuracy, the Major, Max Feret, and PerEquivD methods perform better than other methods for both quartz (over 11 samples >50% and 7 samples >70%) and lithics (over 12 samples >50% and 6 samples >70%) (Fig. 7C–D).

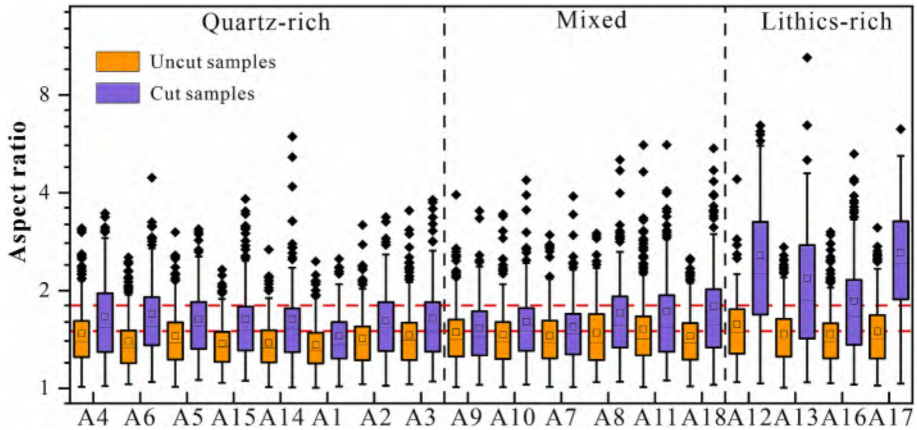

Fig. 11. Aspect ratios of all grains of analyzed samples. Aspect ratio is calculated as the ratio of the major to the minor axis of the best-fit ellipse.

5. Discussion

5.1. The influence of pretreatment procedure to grain texture quantification

Unconsolidated sediments can be imaged directly using binocular or polarizing microscopes without cutting, whereas sandstones are typically cut into thin sections for microscopic analysis. However, the extent to which cutting affects grain texture quantification remains unclear. Here, we compare the results from cut and uncut samples to evaluate the influence of sample preparation on grain-texture measurements, aiming to provide insights that can improve the textural analysis of deep-time consolidated sandstones.

Pretreatment methods influence grain orientation during mounting or sectioning, and thus affect the two-dimensional projections used for grain texture measurements and the resulting quantitative parameters (Fig. 12) (Xie et al., 2020; Anusree and Latha, 2023). In uncut samples, grains tend to rest in their most stable orientations, yielding projections that approximate the maximum particle dimension (Anusree and Latha, 2023). Consequently, the long and short axes of grain projections may represent the longest and intermediate axes of the 3D particles. In contrast, during thin-section preparation, the cutting orientation intersects grains at arbitrary orientations producing projections that vary widely in size and shape and are generally smaller than those obtained from uncut grains (Xie et al., 2020; Anusree and Latha, 2023). As a result, grain sizes derived from cut samples are systematically underestimated relative to those from uncut samples. Mesh sieving primarily constrains the intermediate and minimum particle dimensions (Altuhafi et al., 2013; Wang et al., 2022). Accordingly, when the uncut method is used, grain size descriptors that approximate the intermediate axis, such as the ESD, Minor, Width, and Min Feret methods, show the best agreement with sieve sizes. Consistent with this, Altuhafi et al. (2013) reported that the Min Feret size distribution most closely matches sieve data. Similar findings have also been reported for measurements of gravel and marine calcareous sands (Kumara et al., 2012; Li et al., 2021). By contrast, descriptors based on the longest projected dimension (e.g., the Major and Max Feret) are more appropriate for cut samples. We infer that the reduction in grain projections induced by thin-sectioning leads to an underestimation of the intermediate axis when using the ESD, Minor, Width, and Min Feret methods. Conversely, descriptors targeting the longest projected axis better approximate the true intermediate dimension of grains in thin sections. In addition, we attribute the higher sorting values obtained from cut samples to the random grain projections produced during sectioning (Anusree and Latha, 2023). Thus, sediment sorting may be systematically overestimated when using the cut pretreatment method.

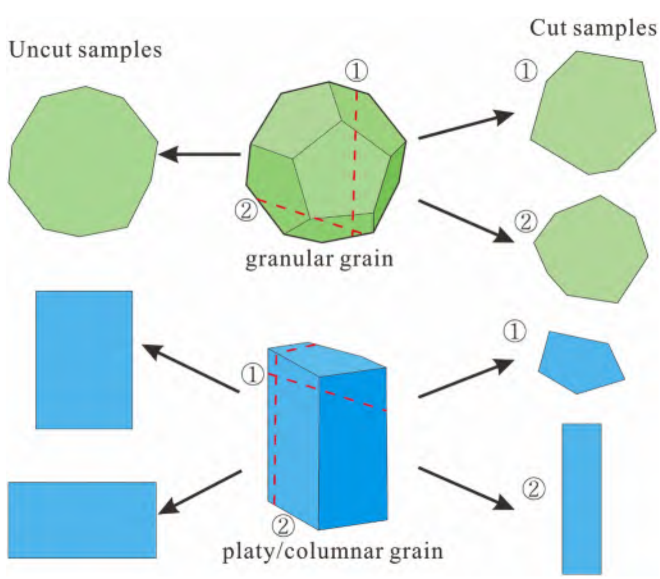

Fig. 12. Schematic illustration showing the influence of the uncut and cut methods on the two-dimensional projection of particle grains. When using the uncut method, the largest projection of the particle grain is obtained. Grain projections are random with various shapes and sizes when using the cut method. The cut projections of granular grains are commonly smaller than uncut projections. The cut shapes of platy or columnar grains may be distinct. The aspect ratio of platy grains may be overestimated when the cutting orientation is perpendicular to the largest face of the grain. Red dashed lines mark the cutting orientations.

Our results demonstrate that the cut method systematically reduces grain projections of sediment grains and thereby biases size quantification (Figs. 5, 6). Hence, grain size measurements from sandstone thin sections should be corrected to better approximate true 3D grain parameters. Previous studies have combined 2D and 3D analyses to establish empirical relationships between 2D projections and 3D textural parameters (Zheng et al., 2019; Xie et al., 2020; Li and Iskander, 2021; Beemer et al., 2022). For example, Garefalakis et al. (2023) proposed correcting grain size distributions by increasing D_{16}, D_{50}, and D_{84} by approximately 17%. Zheng et al. (2019) and Xie et al. (2020) derived linear relationships between 2D and 3D textural parameters, using the largest projected area and the mean of the three largest projected areas, respectively. Although the resulting coefficients differ slightly, both are close to 1. In this study, we therefore treat the grain sizes obtained from uncut projections as alternative 3D grain sizes. Four samples, including A5, A7, A13, and A18, were selected to evaluate the relationship between 2D data and 3D data. Considering the influence of lithologies and depositional settings, four chosen samples include river sand, beach sand, and continental shelf sand, and compositionally span quartz-rich, mixed, and lithics-rich sands. We then compared the size distributions of these four samples treated by the uncut method with corrected cut sizes multiplied by different factors (Fig. 13). The results indicate that corrected cut sizes of the cut grains show good agreement with uncut sizes when multiplied by factors of 1.15–1.25, although the optimal coefficient varies with quantification metric and sample type. Overall, grain sizes derived from cut samples are commonly underestimated and should be corrected by a factor of approximately 1.15–1.25 to better represent true grain dimensions in sandstones. This correction can be beneficial for paleoenvironmental reconstruction based on sandstone textural features. We acknowledge, however, that these correlation factors were established based on 2D data from uncut and cut methods without solid evidence from 3D measurement. Further validation using direct 3D measurements (e.g., μCT) on a wider range of sediment types is therefore necessary in future studies.

When using the Wadell's method, roundness quantified by digital image processing is related to the outlines of particles (Takashimizu and Iiyoshi, 2016). In contrast, the Pentland's roundness is related to the shape of the particle projection. According to the definition of the Pentland's roundness, the larger the maximum axis of a particle grain, the lower the Pentland's roundness, indicating that grains with high aspect ratio tend to yield low Pentland's roundness values. This phenomenon is particularly evident in the lithics-rich samples, which are mainly composed of platy metasedimentary lithics (Fig. 5G–I). The aspect ratios of these grains are significantly higher after thin sectioning compared with uncut grains (Fig. 11). Consequently, the Pentland's roundness is generally lower when using the cut method, especially for lithics-rich samples.

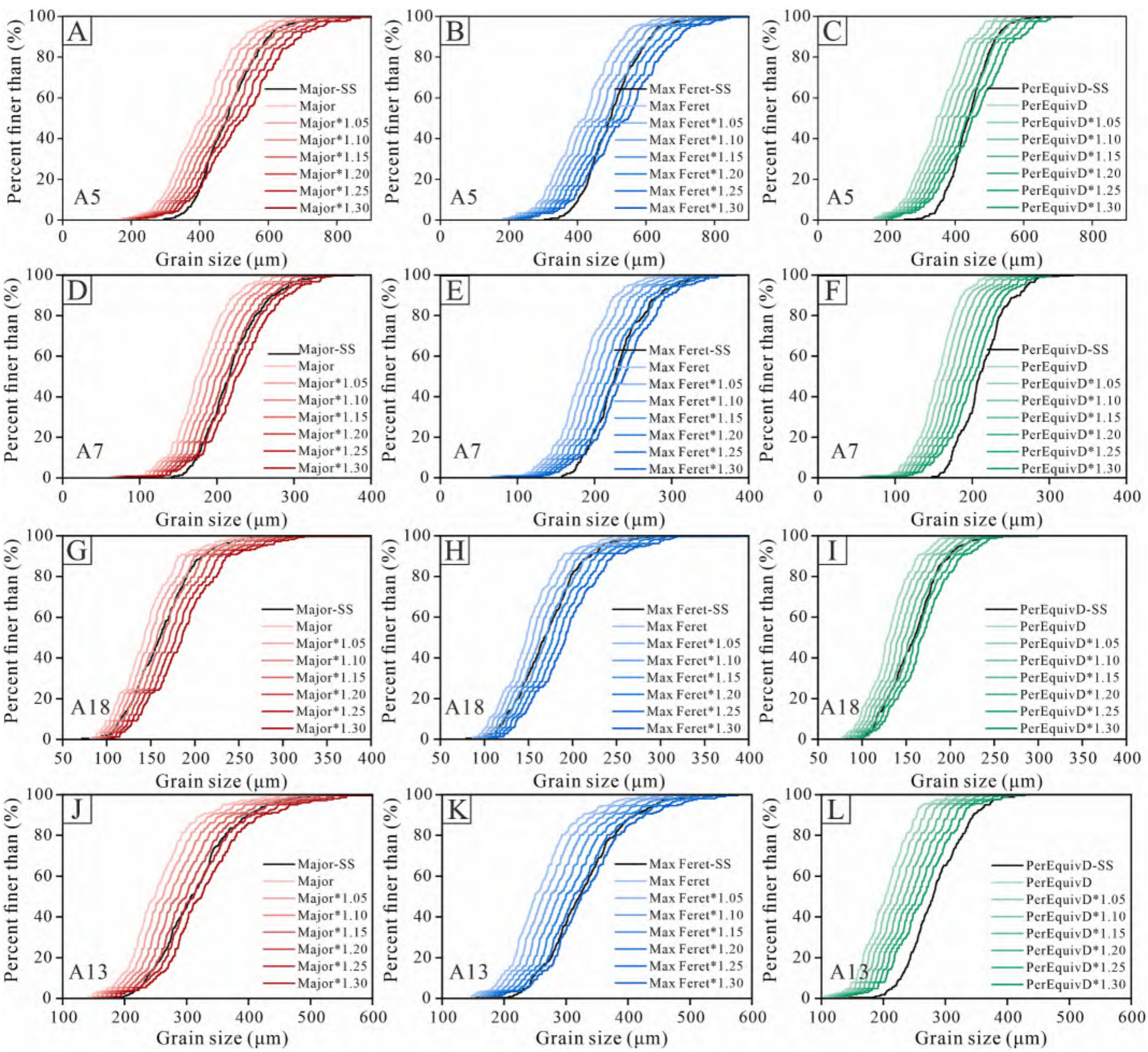

Fig. 13. Cumulative distribution curves of grain sizes of samples A5 (A–C), A7 (D–F), A18 (G–I), and A13 (J–L). These four samples include quartz-rich, mixed, and lithics-rich samples. The left panel shows Length size, the middle panel shows Major size, and the right panel shows Max Feret size. Black lines represent curves of uncut sizes, and colored lines represent corrected cut sizes with different coefficients (from 1.05 to 1.30 at intervals of 0.05).

5.2. The influence of grain shape to grain texture quantification

Detrital grains can exhibit markedly different shapes, such as granular quartz grains and platy low-grade metasedimentary lithic fragments. In this section, we compare the quantification results of quartz and lithic grains to evaluate the influence of grain shape on grain textural quantification results. For consistency and because it allows simultaneous compositional and textural analysis, we restrict this comparison to quartz and lithic grains prepared using the cut method.

The observation that the same methods perform well for both quartz and lithic grains is expected, given that shape differences between quartz and lithics are only pronounced in platy metasedimentary lithics-rich samples (Fig. 11). The shape of detrital grains can influence grain size quantification results (Varga et al., 2018). To evaluate this effect, we categorized all analyzed grains into four groups based on aspect ratio, i.e., 1–1.5, 1.5–1.8, 1.8–2.5, and > 2.5, and compared the accuracy of each method across these four groups. According to aspect ratio, rod, branch, and blade grains can be distinguished from spherical or disk grains (Zheng et al., 2019; Wang et al., 2022). The results show that all methods except MinR exhibit relatively high accuracy (approximately 70%) for grains with aspect ratios of 1–1.5 (spherical or disk grains). As aspect ratio increases, accuracy declines across all methods (Fig. 14). The ESD, Width, Minor, Min Feret, and ArEquivD methods are less influenced by grain aspect ratio than the Length, Major, Max Feret, and PerEquivD methods (Fig. 14). This phenomenon indicates that methods measuring the largest dimension of a particle are more sensitive to particle shape, particularly yielding lower accuracy for blade or platy particles (aspect ratio larger than 1.5). This discrepancy arises because the longest axis of particles with a high aspect ratio is substantially longer than the intermediate axis, and thus exceeds the sieve-derived grain size. For spherical or granular grains, the longest and intermediate axes are approximately equal (Fig. 12). Consequently, all quantification methods show similar accuracy for low aspect ratio grains. For cut samples, the Length, Major, Max Feret, and PerEquivD methods are characterized by relatively high accuracy (approximately 60%) and are barely influenced by aspect ratio. In contrast, other methods are strongly affected by aspect ratio and exhibit lower accuracy (Fig. 14). The shape and size of grain projections can be substantially altered after thin sectioning, especially for platy grains (Fig. 12). The weak influence of aspect ratio on methods measuring the long axis of grain projections indicates that grain shape has little effect on size quantification when these methods are used. Conversely, the short axes of grain projections are commonly smaller than the mesh size, particularly for grains with high aspect ratios. As a result, methods based on short axis measurements show lower accuracy, which is largely controlled by grain aspect ratio.

The shape of detrital grains in sediments is closely related to several factors, including parent-rock lithology, grain composition, mechanical and chemical modification during their sedimentary history, and the sedimentary setting in which the grains deposited (Campaña et al., 2016; Yao and Li, 2023). On one hand, fresh sands derived from crystalline rocks as weathering products, such as decomposed granite soils, have experienced relatively weak modification. Sand grains in soils are commonly characterized by angular outlines and high roughness (Chmielowska et al., 2021; Yao and Li, 2023). On the other hand, grains deposited in high-energy hydrodynamic or aeolian environments, such as beaches and deserts, may experience substantial modification (Garzanti, 2017; Yao and Li, 2023). As a result, grain shapes tend to become more rounded, and their aspect ratios decrease accordingly, such as samples A2 (old red sand; Fig. 5A–C) and A5 (beach sand; Fig. S3A–B). Fluvial transport typically promotes progressive rounding of grain corners through mechanical abrasion. Grains in fluvial sediments also tend to become more rounded and decrease in aspect ratio. However, the degree of modification is comparatively smaller, because hydrodynamic forces are generally less effective than aeolian activity in reshaping grains (Fig. 5; Chmielowska et al., 2021). Detrital grain

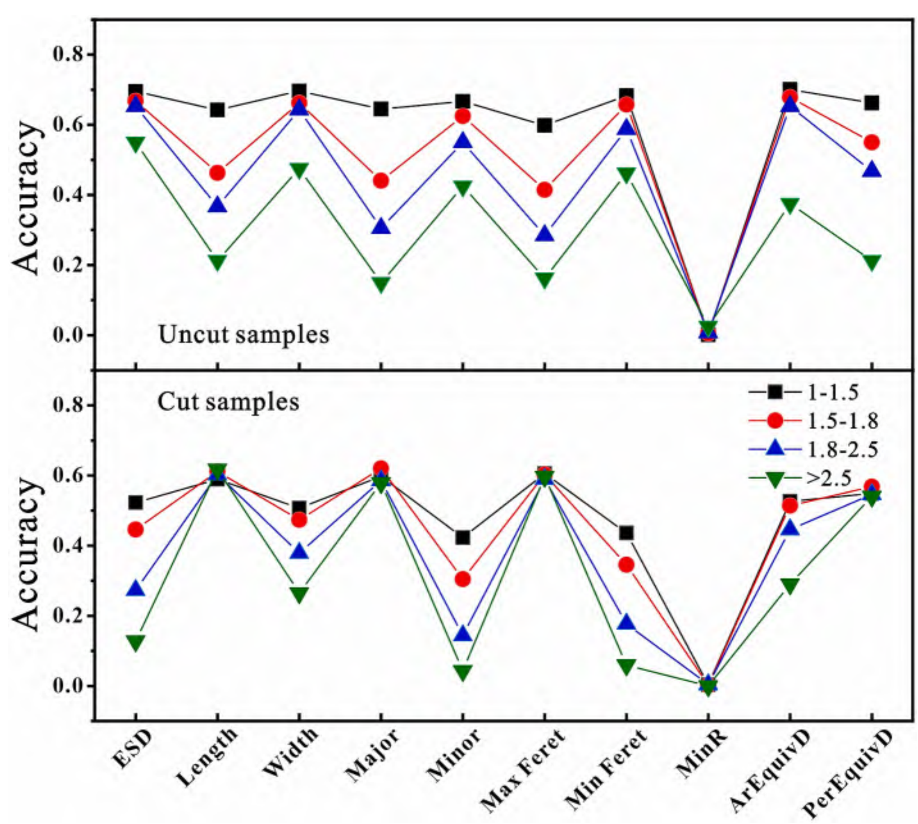

Fig. 14. Comparison of accuracy among different aspect ratio fractions and differences between results of uncut samples (upper panel) and cut samples (lower panel).

composition also plays an important role. Quartz-rich sands with high compositional maturity are mostly spherical or granular, whereas lithics-rich sands derived from shale, slate, and phyllite rocks are predominantly platy or blade-shaped (Fig. 5). In addition to framework grains, grain textural quantification of accessory detrital minerals is also important, especially for minerals widely used in sedimentary provenance analysis, such as zircon, rutile, and garnet (Shen et al., 2024). The shapes of these mineral grains vary significantly. For example, detrital zircon can be granular for recycled grains or elongated columnar for first-cycle grains derived from igneous rocks. Therefore, biases induced by grain shape when quantifying grain texture need further attention.

5.3. Grain texture quantification for unconsolidated sands and sandstones: method selection, recommendations, and a feasible workflow

A comparison of the accuracy of each size metric across different sediment types reveals substantial variations in method performance (Fig. S2). For unconsolidated sands, the ESD, Minor, Min Feret, and ArEquivD methods generally exhibit relatively high accuracy for most sediment types, except for the three old red sand samples (accuracy is typically below 0.4). In contrast, the Major and Max Feret methods show higher accuracies (0.4–0.6). SEM images of sample A2 reveal a broad grain size range (Fig. 5C), consistent with its high sorting index (0.2920). Despite mesh sieving, a substantial proportion of fine-grained particles remains in this sample. In addition, the grains display pronounced surface roughness (Fig. 5C), which likely hinders passage through the sieves, resulting in poorer sorting and lower measurement accuracy. Nevertheless, because old red sands are dominated by granular quartz grains similar to those in beach sands (Fig. 5C; Fig. S3), we infer that the ESD, Minor, Min Feret, and ArEquivD methods remain the most suitable descriptors for this sediment type. For sandstones, the Length, Major, Max Feret, and PerEquivD methods demonstrate high accuracy across most sediment types, except for two quartz-rich continental shelf sand samples. For these two marine sands, the ESD, Minor, and Min Feret methods show higher accuracy (>0.6). SEM images of sample A15 indicate a dominance of coarse granular grains, mostly around 500 μm in size (Fig. S3). Grain projections for this sample are enlarged when the cut method is applied (Fig. 6A), although the reason for this phenomenon remains unclear.

Based on these results, we propose a workflow outlining grain size measurement strategies for commonly analyzed sands and sandstones (Fig. 15). For unconsolidated sandy sediments, such as modern river sands and beach sands, the uncut method is highly recommended because of its relatively high measurement accuracy. Sediments should first be classified by composition into quartz-rich, mixed, and lithics-rich types. Quartz-rich sands, which are dominated by granular grains, are best measured using the ESD, Minor, Min Feret, and ArEquivD methods. Mixed and lithics-rich siliciclastic sands exhibit more variable grain shapes; for riverine and marine sediments, the ESD, Minor, Min Feret, and ArEquivD methods remain appropriate, as these methods are less sensitive to grain shape variation. Furthermore, marine calcareous sands, composed mainly of clastic biogenic carbonate fragments and characterized by highly variable shapes (Li et al., 2021), are inferred to behave similarly to platy lithics-rich sands and can therefore be effectively quantified using the ESD, Minor, and Min Feret methods. Freshly produced sand grains in soils with high surface roughness (Yao and Li, 2023), which are analogous to the old red sands analyzed in this study, are likewise suited to the ESD, Minor, Min Feret, and ArEquivD methods. For sandstones, the cut method provides the most practical pretreatment option. Marine quartz-rich sands are best measured with the ESD, Minor, and Min Feret methods, whereas beach and aeolian quartz-rich sands, along with riverine and marine mixed and lithics-rich sands, can be more reliably quantified using the Major, Max Feret, and PerEquivD methods (Fig. 15).

In conclusion, each of the grain-size quantification methods examined in this study possesses inherent strengths and limitations, and the selection of an appropriate method depends in part on sediment types. Based on their definitions and computational principles, these methods emphasize different dimensions of grain projections. Furthermore, mineralogical composition may also exert some influence on methodology strategy. The MinR method focuses on the minimum inscribed circle of the grain. Because detrital grains are generally irregular, applying this method usually results in an underestimation of grain size; consequently, this approach is commonly used in assessing grain roundness rather than providing absolute grain-size measurements. The Major, Length, Max Feret, and PerEquivD methods are similar, focusing on the longest axis of particle projection. The Minor, Width, Min Feret, ArEquivD methods yield relatively small sizes because these methods focus the intermediate axis of particle projection. For granular grains with low aspect ratios, the longest and intermediate axes are close and results of these methods are thus similar (Fig. 14). However, for grains with high aspect ratios, the results from methods that measure the long and short axes will show considerable differences (Fig. 6). The ESD method comprehensively concerns both the long and short axes of grains, and is widely used in sedimentological researches (Garzanti et al., 2008; Lawrence et al., 2011). However, this method is largely

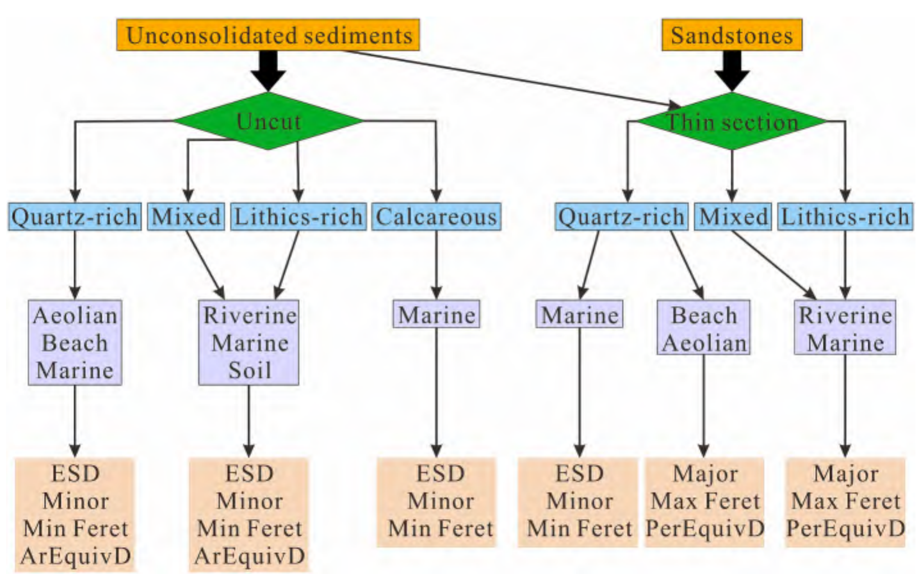

Fig. 15. A workflow chart for selecting sediment grain size quantification methods for different types of sandy sediments.

controlled by the intermediate length of particle and may underestimate grain size for elongated grains with high aspect ratios (Fig. 6C; Fig. 14). Consequently, the selection of quantification method should be adapted to the sample preparation approaches (Fig. 15). In practice, however, the application of a standardized method for grain-size determination is advantageous for achieving robust inter-sample comparability. We suggest that, when sand petrographic composition is not considered, the ESD method is suitable for uncut grains and the method Max Feret is suitable for cut grains.

6. Conclusions and perspectives

Two-dimensional digital image processing has been widely used to quantify grain textural parameters of both unconsolidated sands and sandstones. In this study, a comparative analysis of measurement data obtained through ten grain size descriptors and two roundness quantification methods allows us to evaluate the influences of sample pretreatment and grain shape on textural quantification. Grain sizes obtained from cut samples (thin sections) are generally smaller than those from uncut samples. This discrepancy arises because uncut grains theoretically yield their maximum projection, whereas cut grains are sectioned at random orientations, producing generally smaller sizes. Measurements of grain roundness and sediment sorting are also dependent on the pretreatment methods. Furthermore, grain shape exerts a primary control on size measurement accuracy. Specifically, higher grain aspect ratios (larger than 1.8) lead to lower quantification accuracy across all methods. This study advances grain textural quantification for ancient sandstones based on thin sections, and provides useful insights for paleoenvironment reconstruction using coarse-grained sedimentary records and for sandstone hydrocarbon reservoir characterization. A workflow incorporating a method selection strategy was established to guide grain textural quantification in both unconsolidated sands and sandstones, which can facilitate further investigation of sand-sized sedimentary records in various disciplines of geosciences.

CRediT authorship contribution statement

Xiaotian Shen: Writing – original draft, Visualization, Methodology, Investigation, Formal analysis, Data curation, Conceptualization. **Xing Jian:** Writing – review & editing, Supervision, Resources, Methodology, Investigation, Funding acquisition, Data curation, Conceptualization. **Wei Zhang:** Writing – review & editing, Resources, Investigation, Funding acquisition, Conceptualization. **Ruolan Liao:** Writing – review & editing, Visualization, Methodology, Formal analysis, Data curation. **Dongming Hong:** Writing – review & editing, Methodology, Investigation, Formal analysis, Data curation. **Chao Li:** Writing – review & editing, Resources, Investigation. **Shaohua Zhao:** Writing – review & editing, Resources, Investigation. **James T. Liu:** Writing – review & editing, Methodology, Investigation. **Yuan-Pin Chang:** Writing – review & editing, Methodology, Investigation.

Declaration of competing interest

The authors declare that they have no known competing financial interests or personal relationships that could have appeared to influence the work reported in this paper.

Acknowledgements

This study was funded by the National Natural Science Foundation of China (Nos. 42476051, 41806052) and the Natural Science Foundation of Xiamen, China (No. 3502Z20227006). We thank Hanghai Liang, Shuo Zhang, Haowei Mei for their help with sampling. We sincerely thank the Editor-in-Chief, Dr. Catherine Chagué, the reviewer Dr. Koushik Saha, and another anonymous reviewer for their constructive comments and suggestions, which have substantially improved our manuscript.

Appendix A. Supplementary data

Supplementary data to this article can be found online at https://doi.org/10.1016/j.sedgeo.2026.107186.

Data availability

The data that supports the findings of this study are available in the supplementary material of this article.

References

Altuhafi, F.N., O'Sullivan, C., Cavarretta, I., 2013. Analysis of an image-based method to quantify the size and shape of sand particles. Journal of Geotechnical and Geoenvironmental Engineering 139 (8), 1290–1307. https://doi.org/10.1061/(ASCE)GT.1943-5606.0000855.

Altuhafi, F.N., Coop, M.R., Georgiannou, V.N., 2016. Effect of particle shape on the mechanical behavior of natural sands. Journal of Geotechnical and Geoenvironmental Engineering 142 (12), 04016071. https://doi.org/10.1061/(ASCE)GT.1943-5606.0001569.

Anusree, K.V., Latha, G.M., 2023. Characterization of sand particle morphology: state-of-the-art. Bulletin of Engineering Geology and the Environment 82 (7), 269. https://doi.org/10.1007/s10064-023-03309-x.

Bagheri, G.H., Bonadonna, C., Manzella, I., Vonlanthen, P., 2015. On the characterization of size and shape of irregular particles. Powder Technology 270, 141–153. https://doi.org/10.1016/j.powtec.2014.10.015.

Beemer, R.D., Li, L., Leonti, A., Shaw, J., Fonseca, J., Valova, I., Iskander, M., Pilskaln, C. H., 2022. Comparison of 2D optical imaging and 3D microtomography shape measurements of a coastal bioclastic calcareous sand. Journal of Imaging 8 (3), 72. https://doi.org/10.3390/jimaging8030072.

Campaña, I., Benito-Calvo, A., Pérez-González, A., De Castro, J.B., Carbonell, E., 2016. Assessing automated image analysis of sand grain shape to identify sedimentary facies, Gran Dolina archaeological site (Burgos, Spain). Sedimentary Geology 346, 72–83. https://doi.org/10.1016/j.sedgeo.2016.09.010.

Chmielowska, D., Woronko, B., Dorocki, S., 2021. Applicability of automatic image analysis in quartz-grain shape discrimination for sedimentary setting reconstruction. Catena 207, 105602. https://doi.org/10.1016/j.catena.2021.105602.

Cox, M.R., Budhu, M., 2008. A practical approach to grain shape quantification. Engineering Geology 96 (1–2), 1–16. https://doi.org/10.1016/j.enggeo.2007.05.005.

Deal, E., Venditti, J.G., Benavides, S.J., Bradley, R., Zhang, Q., Kamrin, K., Perron, J.T., 2023. Grain shape effects in bed load sediment transport. Nature 613 (7943), 298–302. https://doi.org/10.1038/s41586-022-05564-6.

Dickinson, W.R., 1985. Interpreting provenance relations from detrital modes of sandstones. In: Zuffa, G.G. (Ed.), Provenance of Arenites. Springer, Netherlands, pp. 333–361.

Dickinson, W.R., Suczek, C.A., 1979. Plate tectonics and sandstone compositions. American Association of Petroleum Geologists Bulletin 63 (12), 2164–2182. https://doi.org/10.1306/2F9188FB16CE-11D7-8645000102C1865D.

Folk, R.L., 1980. Petrology of Sedimentary Rocks. Hemphill Publishing Co, USA, p. 182.

Garefalakis, P., do Prado, A.H., Mair, D., Douillet, G.A., Nyffenegger, F., Schlunegger, F., 2023. Comparison of three grain size measuring methods applied to coarse-grained gravel deposits. Sedimentary Geology 446, 106340. https://doi.org/10.1016/j.sedgeo.2023.106340.

Garzanti, E., 2017. The maturity myth in sedimentology and provenance analysis. Journal of Sedimentary Research 87 (4), 353–365. https://doi.org/10.2110/jsr.2017.17.

Garzanti, E., Andò, S., Vezzoli, G., 2008. Settling equivalence of detrital minerals and grainsize dependence of sediment composition. Earth and Planetary Science Letters 273 (1–2), 138–151. https://doi.org/10.1016/j.epsl.2008.06.020.

Garzanti, E., Andò, S., Vezzoli, G., 2009. Grain-size dependence of sediment composition and environmental bias in provenance studies. Earth and Planetary Science Letters 277 (3–4), 422–432. https://doi.org/10.1016/j.epsl.2008.11.007.

Hamzeloo, E., Massinaei, M., Mehrshad, N., 2014. Estimation of particle size distribution on an industrial conveyor belt using image analysis and neural networks. Powder Technology 261, 185–190. https://doi.org/10.1016/j.powtec.2014.04.038.

Hong, D., 2020. Provenance of the Old Red Sand in coastal zones of southeast China and its implications for climate and land-sea interaction during the late Pleistocene (Master Thesis). Xiamen University, China.

Houghton, J.E., Behnsen, J., Duller, R.A., Nichols, T.E., Worden, R.H., 2024. Particle size analysis: A comparison of laboratory-based techniques and their application to geoscience. Sedimentary Geology 464, 106607. https://doi.org/10.1016/j.sedgeo.2024.106607.

Huang, C.Y., 2017. Geological ages of Taiwan stratigraphy and tectonic events. Scientia Sinica Terrae 47 (4), 394–405. https://doi.org/10.1360/n072017-00023 (In Chinese with English abstract).

Institute of Geology, 2002. Chinese Academy of Geological Sciences. Geological Atlas of China.

Jin, J., Li, Z., Lei, G., Ling, Y., Jiang, F., Shen, J., Liu, X., 2017. Chronology and environmental significance of old red sand in South China: take the old red sand in

Qingfeng, Fujian as an example. Scientia Geographica Sinica 37 (2), 301–310. https://doi.org/10.13249/j.cnki.sgs.2017.02.017 (In Chinese with English abstract).
Konert, M., Vandenberghe, J.E.F., 1997. Comparison of laser grain size analysis with pipette and sieve analysis: a solution for the underestimation of the clay fraction. Sedimentology 44 (3), 523–535.
Kumara, G.J.J., Hayano, K., Ogiwara, K., 2012. Image analysis techniques on evaluation of particle size distribution of gravel. International Journal of GEOMATE 3 (5), 290–297.
Lawrence, R.L., Cox, R., Mapes, R.W., Coleman, D.S., 2011. Hydrodynamic fractionation of zircon age populations. Geological Society of America Bulletin 123 (1–2), 295–305. https://doi.org/10.1130/b30151.1.
Li, L., Iskander, M., 2021. Comparison of 2D and 3D dynamic image analysis for characterization of natural sands. Engineering Geology 290, 106052. https://doi.org/10.1016/j.enggeo.2021.106052.
Li, L., Beemer, R.D., Iskander, M., 2021. Granulometry of two marine calcareous sands. Journal of Geotechnical and Geoenvironmental Engineering 147 (3), 04020171. https://doi.org/10.1061/(ASCE)GT.1943-5606.0002431.
Li, L., Sun, Q., Iskander, M., 2023. Efficacy of 3D dynamic image analysis for characterising the morphology of natural sands. Géotechnique 73 (7), 586–599. https://doi.org/10.1680/jgeot.21.00128.
Li, Z., Qiu, J.S., Yang, X.M., 2014. A review of the geochronology and geochemistry of Late Yanshanian (Cretaceous) plutons along the Fujian coastal area of southeastern China: implications for magma evolution related to slab break-off and rollback in the Cretaceous. Earth-Science Reviews 128, 232–248. https://doi.org/10.1016/j.earscirev.2013.09.007.
Ludwick, J.C., Henderson, P.L., 1968. Particle shape and inference of size from sieving. Sedimentology 11 (3–4), 197–235.
Mazzullo, J., Ritter, C., 1991. Influence of sediment source on the shapes and surface textures of glacial quartz sand grains. Geology 19 (4), 384–388.
Muhlbauer, J.G., Fedo, C.M., Farmer, G.L., 2017. Influence of textural parameters on detrital-zircon age spectra with application to provenance and paleogeography during the Ediacaran–Terreneuvian of southwestern Laurentia. GSA Bulletin 129 (11−12), 1585–1601. https://doi.org/10.1130/B31611.1.
Murtaza, G., Ali, N., Hussain, W., Iqbal, S.M., Azhar, M.U., Ahmad, T., Iitaf, K.H., Ahmed, A., 2025. Integrating petrophysical, seismic and rock physics analyses for precise reservoir characterization. Earth Systems and Environment 1–23. https://doi.org/10.1007/s41748-025-00654-7.
Payton, R.L., Chiarella, D., Kingdon, A., 2022. The influence of grain shape and size on the relationship between porosity and permeability in sandstone: a digital approach. Scientific Reports 12 (1), 7531. https://doi.org/10.1038/s41598-022-11365-8.
Pentland, A., 1927. A method of measuring the angularity of sands. Proceedings and Transactions of the Royal Society of Canada 21 (3), 43.
Perlo, J., Mülder, C., Danieli, E., Hopmann, C., Blümich, B., Casanova, F., 2016. Digital processing of images of extruded rubber profiles for process control MRI. Measurement 82, 466–475. https://doi.org/10.1016/j.measurement.2015.11.046.
Resentini, A., Andò, S., Garzanti, E., 2018. Quantifying roundness of detrital minerals by image analysis: sediment transport, shape effects, and provenance implications. Journal of Sedimentary Research 88 (2), 276–289. https://doi.org/10.2110/jsr.2018.12.
Reynolds, T., 2024. Grain size from source to sink–modern and ancient fining rates. Earth-Science Reviews 250, 104699. https://doi.org/10.1016/j.earscirev.2024.104699.
Rubey, W.W., 1933. The size distribution of heavy minerals within a water-laid sandstone. Journal of Sedimentary Research 3 (1), 3–29.
Shang, Y., Kaakinen, A., Beets, C.J., Prins, M.A., 2018. Aeolian silt transport processes as fingerprinted by dynamic image analysis of the grain size and shape characteristics of Chinese loess and Red Clay deposits. Sedimentary Geology 375, 36–48. https://doi.org/10.1016/j.sedgeo.2017.12.001.
Shen, X., Jian, X., Li, C., Liu, J.T., Chang, Y.-P., Zhang, S., Mei, H., Fu, H., Zhang, W., 2021. Submarine topography-related spatial variability of the southern Taiwan Strait sands (East Asia). Marine Geology 436, 106495. https://doi.org/10.1016/j.margeo.2021.106495.
Shen, X., Jian, X., Zhang, W., Guan, P., 2024. Grain textural bias in detrital single-mineral provenance studies. Sedimentary Geology 471, 106731. https://doi.org/10.1016/j.sedgeo.2024.106731.
Shen, X., Jian, X., Zhang, W., Ye, S., Liang, H., Zhuang, Y., Guan, P., 2025. Cenozoic sandstone provenance in the Qaidam Basin of China, and its implications for the deformation history of the Tibetan Plateau. Palaeogeography Palaeoclimatology Palaeoecology 675, 113120. https://doi.org/10.1016/j.palaeo.2025.113120.
Sochan, A., Zieliński, P., Bieganowski, A., 2015. Selection of shape parameters that differentiate sand grains, based on the automatic analysis of two-dimensional images. Sedimentary Geology 327, 14–20. https://doi.org/10.1016/j.sedgeo.2015.07.007.
Sun, Y., Indraratna, B., Nimbalkar, S., 2014. Three-dimensional characterisation of particle size and shape for ballast. Géotechnique Letters 4 (3), 197–202. https://doi.org/10.1680/geolett.14.00036.
Takashimizu, Y., Iiyoshi, M., 2016. New parameter of roundness R: circularity corrected by aspect ratio. Progress in Earth and Planetary Science 3 (1), 2. https://doi.org/10.1186/s40645-015-0078-x.
Újvári, G., Kok, J.F., Varga, G., Kovács, J., 2016. The physics of wind-blown loess: Implications for grain size proxy interpretations in Quaternary paleoclimate studies. Earth-Science Reviews 154, 247–278. https://doi.org/10.1016/j.earscirev.2016.01.006.
Vandel, E., Vaasma, T., Sugita, S., 2020. Application of image analysis technique for measurement of sand grains in sediments. MethodsX 7, 100981. https://doi.org/10.1016/j.mex.2020.100981.
Vandenberghe, J., 2013. Grain size of fine-grained windblown sediment: A powerful proxy for process identification. Earth-Science Reviews 121, 18–30. https://doi.org/10.1016/j.earscirev.2013.03.001.
Vandenberghe, J., Sun, Y., Wang, X., Abels, H.A., Liu, X., 2018. Grain-size characterization of reworked fine-grained aeolian deposits. Earth-Science Reviews 177, 43–52. https://doi.org/10.1016/j.earscirev.2017.11.005.
Varga, G., Kovács, J., Szalai, Z., Cserháti, C., Újvári, G., 2018. Granulometric characterization of paleosols in loess series by automated static image analysis. Sedimentary Geology 370, 1–14. https://doi.org/10.1016/j.sedgeo.2018.04.001.
Wadell, H., 1932. Volume, shape and roundness of rock particles. Journal of Geology 40, 443–451.
Wang, L., Jian, X., Mei, H., Shen, X., Fu, H., 2024. Clay composition heterogeneity in sediments from mountainous catchments with contrasting bedrock lithology in SE China coast. Catena 247, 108470. https://doi.org/10.1016/j.catena.2024.108470.
Wang, X., Wang, Y., Liao, C., Cui, J., Shen, J.H., Wang, X.Z., Zhu, C.Q., 2022. Particle breakage mechanism and particle shape evolution of calcareous sand under impact loading. Bulletin of Engineering Geology and the Environment 81 (9), 372. https://doi.org/10.1007/s10064-022-02868-9.
Weltje, G.J., von Eynatten, H., 2004. Quantitative provenance analysis of sediments: review and outlook. Sedimentary Geology 171 (1–4), 1–11. https://doi.org/10.1016/j. sedgeo.2004.05.007.
Woronko, B., Dłużewski, M., Woronko, D., 2017. Sand-grain micromorphology used as a sediment-source indicator for Kharga Depression dunes (Western Desert, S Egypt). Aeolian Research 29, 42–54. https://doi.org/10.1016/j.aeolia.2017.10.001.
Wu, M., Xiong, L., Wang, J., 2021. DEM study on effect of particle roundness on biaxial shearing of sand. Underground Space 6 (6), 678–694. https://doi.org/10.1016/j.undsp.2021.03.006.
Xie, W.Q., Zhang, X.P., Yang, X.M., Liu, Q.S., Tang, S.H., Tu, X.B., 2020. 3D size and shape characterization of natural sand particles using 2D image analysis. Engineering Geology 279, 105915. https://doi.org/10.1016/j.enggeo.2020.105915.
Xu, Y., Sun, Q., Yin, X., Long, H., Li, D., Lin, F., 2024. Late Pleistocene sea level change and tectonism control on the formation of the Old Red Sand along the southeastern coast of China. Palaeogeography Palaeoclimatology Palaeoecology 637, 112018. https://doi.org/10.1016/j.palaeo.2024.112018.
Yan, Y., Zhang, L., Luo, X., Liu, K., Jia, T., Lu, Y., 2023. Influence of the grain shape and packing texture on the primary porosity of sandstone: Insights from a numerical simulation. Sedimentology 70 (6), 1856–1885. https://doi.org/10.1111/sed.13098.
Yang, R.J., Liu, J.T., Fan, D., Burr, G.S., Lin, H.L., Chen, T.T., 2017. Land-sea duel in the late Quaternary at the mouth of a small river with high sediment yield. Journal of Asian Earth Sciences 143, 59–76. https://doi.org/10.1016/j.jseaes.2017.03.028.
Yao, T., Li, W., 2023. Quantifying the particle shape and surface roughness of sands. Bulletin of Engineering Geology and the Environment 82 (4), 135. https://doi.org/10.1007/s10064-023-03167-7.
Zhang, S., Jian, X., Liu, J.T., Wang, P., Chang, Y.P., Zhang, W., 2022. Climate-driven drainage reorganization of small mountainous rivers in Taiwan (East Asia) since the last glaciation: The Zhuoshui River example. Palaeogeography Palaeoclimatology Palaeoecology 586, 110759. https://doi.org/10.1016/j.palaeo.2021.110759.
Zheng, W., Hu, X., Tannant, D.D., Zhang, K., Xu, C., 2019. Characterization of two-and three-dimensional morphological properties of fragmented sand grains. Engineering Geology 263, 105358. https://doi.org/10.1016/j.enggeo.2019.105358.